

**ADAPTATION OF DIGITAL ELECTRONIC INTO
DETECTOR SYSTEMS NUMEXO2 IN EXOTIC
NUCLEI RESEARCH**

**A Thesis Submitted to
the Graduate School of Engineering and Sciences of
İzmir Institute of Technology
in Partial Fulfillment of the Requirements for the Degree of**

MASTER OF SCIENCE

in Physics

**by
Elif ŞAHİN**

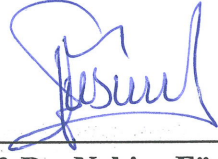
**July 2017
İZMİR**

We approve the thesis of **Elif ŞAHİN**

Examining Committee Members:



Prof. Dr. Durmuş Ali DEMİR
Department of Physics, İzmir Institute of Technology




Prof. Dr. Nebiye Füsün ÇAM
Department of Physics, Ege University

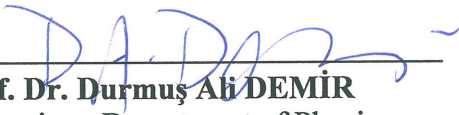


Assoc. Prof. Dr. Devrim Alev GÜÇLÜ
Department of Physics, İzmir Institute of Technology


26 July 2017



Prof. Dr. Sefa ERTÜRK
Co-Supervisor, Department of
Physics, Niğde Ömer Halis Demir
University



Prof. Dr. Durmuş Ali DEMİR
Supervisor, Department of Physics,
İzmir Institute of Technology



Prof. Dr. R. Tuğrul SENGER
Head of the Department of Physics

Prof. Dr. Aysun SOFUOĞLU
Dean of Graduate School of
Engineering and Sciences

ACKNOWLEDGMENTS

First of all, it is an honor for me to thank my co-advisor Prof. Dr. Sefa Ertürk, who guided me throughout my research with patience, understanding and much encouragement. I also want to thank him for not only giving me the opportunity to study nuclear physics, but for his support in allowing me to travel and attend many activities. I have gained priceless knowledge thanks to him. And also, I would like to express my deepest gratitude to his wife Tülin Ertürk for hospitality.

Also, I would like to thank Research Assistant Dr. Bahadır Sayğı for giving me the chance to study in this field. I am so grateful to him for his support, much valuable help, coffee, and discussions.

I would like to thank the members of committee Prof. Dr. Durmuş Ali Demir, Assoc. Prof. Dr. Devrim Alev Güçlü and Prof. Dr. Nebiye Füsün Çam for their contribution.

My warmest thanks go to my close friends İlhan Efendioğlu and Tuğçe İşler for their friendship, fun, support, having chats and numerous other things. Without them, the completion of this study would not have been possible.

I would like to thank my friends Hemza Azri, Kemal Gültekin, Beyhan Pulıçe, Jülide Yıldırım, Sevil Altuğ, Emine Bakali, Hazan Özkan, Onur Rauf Yılmaz, Gündoğdu Şahin, Abdurrahman Menaf Altıntaş, Halis Güzelaydın, Kıvanç Uyanık, Zafer Kandemir, Korhan Ertan Çakmak, Gökhan Öztarhan, Dilce Özkendir, Begüm Yavaş for their much valuable friendship, aid, and conversations during our coffee breaks.

My deepest gratitude goes to Burak Uzun for his unconditional love, support, patience, and especially for always putting a smile on my face and filling my heart with happiness during 6 years. Without his love and encouragement, this thesis could not have been completed.

I owe the biggest debt to my parents Akın Şahin, Ceyhan Şahin and my sister Çağrı Şahin, and my grandmother Elife Şahin for their love, limitless support, encouragements, and patience. I would like to dedicate this thesis to them.

I would like to thank Scientific and Technological Research Council of Turkey. This work has been supported by TUBITAK with the project number 114F473.

ABSTRACT

ADAPTATION OF DIGITAL ELECTRONIC INTO DETECTOR SYSTEMS NUMEXO2 IN EXOTIC NUCLEI RESEARCH

The main purpose of this thesis is to introduce and show the performance and capabilities of the newly developed digital electronic namely NUMEXO2, which has been tested, coupled with EXOGAM2 (EXOtic GAMma array) detector at GANIL in France. This electronic has been developed due to the necessity of high rate signal transferring capacity when a radioactive ion beam is applied in order to produce exotic nuclei and to understand their nuclear structure. NUMEXO2 will be used both with stable beam and radioactive beam experiment not only to have high rate digital experimental data during the experiment but also will be used to obtain good high resolution both for energy and time. In this thesis, we will try to explain the design, verification, and performance of the NUMEXO2. In order to show the performance of NUMEXO2, we will present the result from test experiment performed in France at GANIL, nuclear research centre.

ÖZET

EGZOTİK ÇEKİRDEK ARAŞTIRMALARINDA DEDEKTÖR SİSTEMLERİ İÇERİSİNDE NUMEXO2 DİJİTAL ELEKTRONİK SİSTEMİNİN ADAPTASYONU

Bu tezin temel amacı, yeni geliştirilen dijital elektronik, yani test edilen NUMEXO2 'nin GANIL'deki EXOGAM2 (EXOtıc GAMma array) dedektörü ile birlikte performans ve yeteneklerini tanıtmak ve göstermektir. Bu elektronik, egzotik çekirdek üretmek ve nükleer yapısını anlamak için radyoaktif iyon demeti uygulandığında yüksek oranlı sinyal aktarma kapasitesinin gerekliliği nedeniyle geliştirildi. NUMEXO2, hem kararlı ışın hem de radyoaktif ışın deneyi ile, deney sırasında yüksek oranda sayısal deneysel verilere sahip olmakla kalmayıp hem enerji hem de zaman için iyi yüksek çözünürlük elde etmek için kullanılacaktır. Bu tezde, NUMEXO2'nin tasarımını, doğrulamasını ve performansını açıklamaya çalışacağız. NUMEXO2'nin performansını göstermek için, nükleer araştırma merkezi olan GANIL'de Fransa'da yapılan test denemesinin sonucunu sunacağız.

TABLE OF CONTENTS

LIST OF FIGURES	viii
LIST OF TABLES	xi
CHAPTER 1. INTRODUCTION	1
CHAPTER 2. GAMMA SPECTROSCOPY AND DETECTION MECHANISMS .	3
2.1. Exotic Nuclei	3
2.2. Gamma-Rays	4
2.3. Processes of Gamma-Ray Interactions with Matter	5
2.3.1. The Photoelectric Effect	6
2.3.2. The Compton scattering	7
2.3.3. Pair Production	8
2.4. Detection of Gamma Rays	10
2.5. Neutron-Matter Interaction Mechanisms	12
CHAPTER 3. FUNDAMENTALS OF SEMICONDUCTOR PHYSICS	14
3.1. Electrical Classification of Solids	14
3.2. Extrinsic and Intrinsic Semiconductors	16
3.2.1. n-type Semiconductors	16
3.2.2. p-Type Semiconductors	18
3.3. The p-n Junction	19
3.4. The High Purity Germanium (HPGe) Radiation Detectors	20
3.5. Energy Resolution	23
CHAPTER 4. THE EXOGAM DETECTOR AND THE NUMEXO2 DIGITIZER .	25
4.1. EXOGAM Detector and Array Design	25
4.1.1. EXOGAM Design Specification	25
4.1.2. Segmented CLOVER Ge detector	26
4.1.3. EXOGAM2 Electronics	29
4.2. The NUMEXO2 Digitizer	31
4.2.1. Definition and Block Diagram of the NUMEXO2 Digitizer	31

4.2.2. The Virtex-6 Block.....	32
4.2.3. The Virtex-5 Block.....	34
4.2.4. Data Readout	34
CHAPTER 5. RESULTS	41
CHAPTER 6. CONCLUSION	52
REFERENCES	53

LIST OF FIGURES

<u>Figure</u>	<u>Page</u>
Figure 2.1. Segré Chart	4
Figure 2.2. Electromagnetic spectrum	5
Figure 2.3. Different gamma rays interactions and the region where they are dominant	6
Figure 2.4. Photoelectric effect and histogram	7
Figure 2.5. Compton scattering	8
Figure 2.6. Histogram of the pair production and energy distribution	9
Figure 2.7. Gamma-rays Spectrum	11
Figure 2.8. Schematic view of neutrons interactions	12
Figure 3.1. (a) The atomic energy levels are discrete lines. (b) In a solid, the allowed energy states become energy bands	15
Figure 3.2. Band structure of solids	15
Figure 3.3. n-type semiconductor	17
Figure 3.4. (a) Intrinsic and (b) n-type semiconductor. New electron states (donor states) are created close to the conduction band	17
Figure 3.5. p-type semiconductor	18
Figure 3.6. (a) Intrinsic and (b) p-type semiconductor. New hole states (acceptor states) are created close to the top of the valence band	19
Figure 3.7. Creation of the depletion region in a p-n junction	20
Figure 3.8. Radiation detection mechanism in a reverse-biased semiconductor	20
Figure 3.9. Configuration of Planar	21
Figure 3.10. Typical arrangement of components in a solid-state detector	22
Figure 3.11. Three common shapes of coaxial detectors. At the bottom shows n-type and p-type geometry and cross section of coaxial detectors	23
Figure 3.12. Response function of the detector in Gaussian shape	24
Figure 4.1. EXOGAM detector array design	26
Figure 4.2. Left: A schematic diagram of the crystals in a segmented CLOVER Ge detector. Right: Zoomed segmented crystal	27
Figure 4.3. The EXOGAM Clover inside its BGO escape suppression shield, consisting of a rear shield to be used in the most compact geometry and an additional side shield to be used for improving the peak-to-total ratio in the pulled-back geometry	28

Figure 4.4. A Cross-section through the 16 segmented CLOVER EXOGAM array .	29
Figure 4.5. Digital electronic system design for EXOGAM2	30
Figure 4.6. NUMEXO2 block diagram	32
Figure 4.7. NUMEXO2 Virtex-6 block diagram	33
Figure 4.8. NUMEXO2 Virtex-5 block diagram	34
Figure 4.9. GECO test and control interface	35
Figure 4.10. Left; NUMEXO2 trigger control panel, Right; Trapezoidal filter slope, K- parameter control panel	36
Figure 4.11. Left; inspection control panel, Right; Oscilloscope control panel	37
Figure 4.12. Left; Trigger timing control panel, Right; K, M ve alfa-parameters control panel	38
Figure 4.13. Left; FADC control panel, Right; Each FADC fine adjustment control panel	38
Figure 4.14. Left; Control panel of data that is acquisition in data registration within parts of NUMEXO2, Right; NUMEXO2 data readout value control panel	39
Figure 4.15. VIGRU graphical interface control panel	40
Figure 5.1. Peaks fitting process of ^{152}Eu radioactive calibration source at 344.785 keV and at 1.408.006 keV.	44
Figure 5.2. Correction coefficients obtained by using energy fitting process by us- ing each of crystals for two EXOGAM2 detectors.	45
Figure 5.3. First four crystals of EXOGAM2 energy spectrum (in the range of 0-500 keV), the left side shows energy spectra that used calibration coefficients and the right side shows energy spectra that used without calibration coefficients.	46
Figure 5.4. Second four crystals of EXOGAM2 energy spectrum (in the range of 0-500 keV), the left side shows energy spectra that used calibration coefficients and the right side shows energy spectra that used without calibration coefficients.	47
Figure 5.5. First four crystals of EXOGAM2 energy spectrum (in the range of 500-1500 keV), the left side shows energy spectra that used calibration coefficients and the right side shows energy spectra that used without calibration coefficients.	48

Figure 5.6. Second four crystals of EXOGAM2 energy spectrum (in the range of 500-1500 keV), the left side shows energy spectra that used calibration coefficients and the right side shows energy spectra that used without calibration coefficients.	49
Figure 5.7. Results of energy fitting process of each EXOGAM crystal at 344.785 keV.	50
Figure 5.8. Results of energy fitting process of each EXOGAM crystal at 1.408.006 keV.	51

LIST OF TABLES

<u>Table</u>		<u>Page</u>
Table 5.1.	Intense energy value of ^{152}Eu radioactive calibration source	42
Table 5.2.	Measured energy value of ^{152}Eu radioactive calibration source	43
Table 5.3.	Energy resolution values of the EXOGAM2 detector crystals.	44

CHAPTER 1

INTRODUCTION

Over the past decades; studies of the nuclear structure have led to many experiments in order to understand properties of the nucleus. Different nuclear isotopes have different properties, such as stability, decay modes, lifetime, deformation, etc. Thus for predictions, from 5000 to 7000 bound nuclei ought to exist in the universe, but our knowledge on these radioactive nuclei is very limited.

To understand the nuclear structure is a challenging process. One of the most widespread technique to observe the nuclear characteristics is the gamma-ray spectroscopy, in other words, since most radioactive sources generate gamma rays, it is a method for detecting and describing gamma-emitting radioactive matters. A detector can determine an unknown radioisotope by describing features of the gamma spectrum and comparing them to known spectra, moreover, it is able to record both the number of incoming gammas and their corresponding energies.

Nowadays, many detector systems progress with novel technology. Due to this reason, the electronics that are used in these detector systems are renewed. In many applications, switching from analog electronic to digital electronic has been done. Some of the main reasons take some advantages as for example energy resolution, performance, peak shape, complex data analysis, etc.

To discover properties of unknown exotic nuclei, the most efficient devices are HP-Ge (High-Purity Germanium) array detectors, such as EUROBALL [1], GAMMASPHERE [2], MINIBALL [3], EXOGAM [4], AGATA [5], GRETINA [6], JUROGAM II [7]. Moreover, these arrays have been used with neutron detectors such as Neutron Shell [8], Neutron Wall [9, 10], NEDA [11, 12], and with ancillary charged particles detectors such as TRACE [13], DIAMANT [14] and EUCLIDES [15].

In this thesis, Chapter 2 aims to introduce basic knowledge of gamma spectroscopy. Exotic nuclei, gamma-ray interactions with the matter as well as detection of gamma-rays and neutron-matter interactions are presented.

Chapter 3 deals with the fundamentals of the semiconductors. Semiconductor devices especially, semiconductor detectors play major roles to understand nuclear structure. Also, we focused on characteristics of high-purity germanium detectors in this chapter.

Chapter 4 makes reference to the EXOGAM array design, describing electron-

ics, structure, and features. Furthermore, NUMEXO2 digitizer, software, block diagram, details of electronics are presented.

Chapter 5 shows the results obtained for EXOGAM2 electronics. Calibration results, energy resolutions for each crystal are calculated.

Finally, Chapter 6, the conclusions of the thesis work are discussed and interpreted.

CHAPTER 2

GAMMA SPECTROSCOPY AND DETECTION MECHANISMS

2.1. Exotic Nuclei

An atom consists of positively charged protons, neutral neutrons and negatively charged electrons in the universe. The nucleus is located at the center of the atom and consists of protons and neutrons. The total mass of protons and neutrons specify the mass of the nuclei.

The nucleons are held together within the nucleus by the strong interaction which means that the nuclear or strong force is the force between protons and neutrons, this force is attractive within extremely short distances and overcomes the electromagnetic force. However, if the number of the nucleus increases, the repulsive effect of the electromagnetic force gets stronger and thus electromagnetic force overcomes the strong force. When more nucleons unbalance binding energy between protons and neutrons, the atom becomes radioactive for this reason nuclei away from stability ought to transform into another one. This process continues until the stable nuclei are reached. In unstable nuclei instability is caused by the low nuclear forces that cannot generate enough binding energy to keep nucleus together.

A nuclear isotope is composed of a nucleus having the same proton number (Z) with a combination of different numbers of neutrons. Stability of an isotope is determined by the neutron/proton (N/Z) ratio. Figure 2.1 shows a chart of nuclei arranged with respect to their proton and neutron numbers, which is called a Segré Chart. It involves the fundamental information about nuclei such as decay modes, half-life, spin, etc. [16]. Segré Chart shows graphical distribution of the different isotopes discovered up until now. In the chart, horizontal and vertical axes denote the neutron and proton numbers, respectively.

In Figure 2.1 black squares are stable which is located between pink and blue regions. On its left, the blue region make reference to the proton-rich nuclei, tend to get

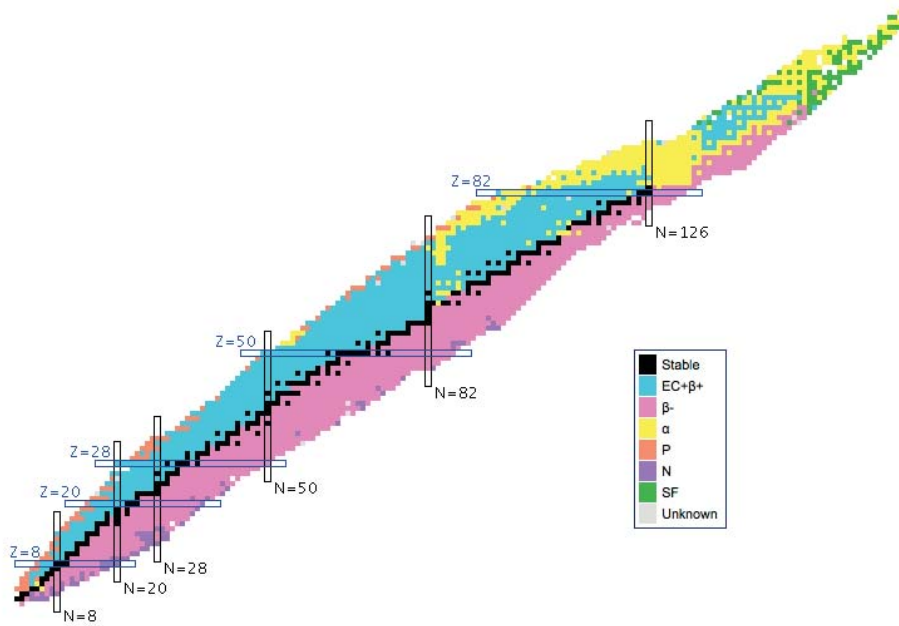


Figure 2.1. Segré Chart [17]

β^+ decay, and on its right, the pink area referred to the neutron rich nuclei, tend to get β^- decay. The yellow region has too high a total of protons or neutrons tend to get α decay. The nuclei that corresponds to green area are tend to undergo spontaneous fission.

Exotic nuclei have greater number of protons and neutrons with respect to stable nuclei. Some of them have more neutrons, while others have more protons. Neutron-rich nuclei try to achieve stable nuclei with beta decay (β^-) which is formed by a neutron turning into a proton, and emitting an electron and an electron neutrino. Likewise, β^+ take place in proton-rich nuclei by turning into a proton to a neutron. N/Z ratio for exotic nuclei is decreased in proton-rich region while N/Z ratio is increased in neutron-rich region with respect to stable nuclei. The alpha particle is a nucleus of the helium element that consists of two protons and two neutrons. In alpha decay, a nucleus emits two protons and two neutrons which mean that the nucleus loses two protons and two neutrons. As a result, the tally of atomic mass decreases by four. In a gamma decay a high energy photon leaves from the nucleus and allows the nucleus to reach a more stable with lower energy configuration. In spontaneous fission process, the nucleus split into nearly equal fragments and one or more neutrons. A large amount of energy is also released.

Segré chart has been not completed, yet. Today, scientists have produced nuclei that has short half-life in the range from nanosecond to femtosecond in laboratories.

Generally, proton rich nuclei are produced with fusion evaporation reaction, neutron rich nuclei are obtained by using fission of actinide nuclides, multi nucleon transfer reactions.

2.2. Gamma-Rays

Gamma-rays refer to electromagnetic radiation (no rest mass, no charge) of a very high energies (Figure 2.2). Gamma rays are high-energy photons with very short wavelengths and thus very high frequency. Gamma rays frequently accompany the emission of alpha and beta radiation.

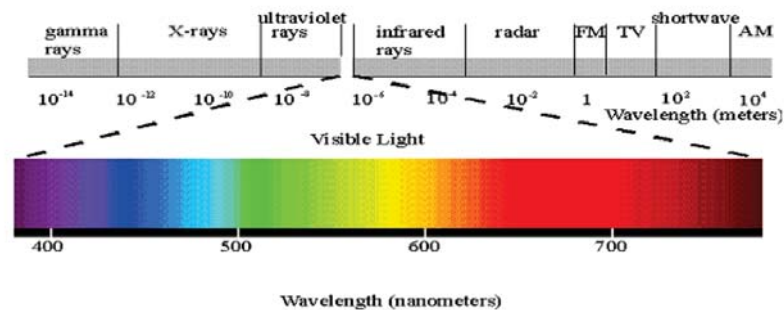


Figure 2.2. Electromagnetic spectrum [18]

Gamma rays are important for nuclear physics because they play an important role to research nuclear structure. Gamma-rays can be generated in different reactions: i) nuclear fusion, ii) nuclear fission, iii) alpha decay, iv) gamma decay.

Nuclear fusion is an atomic reaction in which multiple atoms combine to create a single, more massive atom. The resulting atom has a slightly smaller mass than the sum of the masses of the original atoms.

Nuclear fission is the process in which a large nucleus splits into two smaller nuclei with the release of energy. In other words, fission the process in which a nucleus is divided into two or more fragments, and neutrons and energy are released.

Alpha decay takes place when a heavy nucleus gives off a helium-4 nucleus, reducing its atomic number by 2 and its atomic weight by 4. This process can leave the nucleus with excess energy, which is emitted in the form of a gamma-ray.

Gamma decay occurs when there is too much energy in the nucleus of an atom, causing it to emit a gamma-ray without changing its charge or mass composition.

2.3. Processes of Gamma-Ray Interactions with Matter

Despite the fact that many process of gamma rays interactions are determined, three most significant interactions with matter are that : photoelectric effect, Compton scattering and pair production [16]. These three interactions depend on energy of photons and type of material (atomic number Z) that is used.

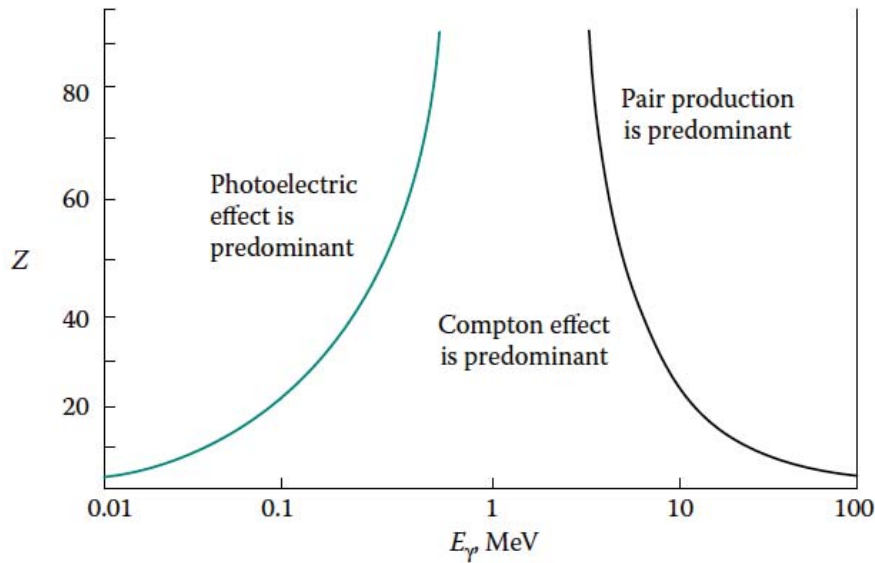


Figure 2.3. Different gamma rays interactions and the region where they are dominant [19]

As can be seen from the Figure 2.3, the areas where these three gamma rays interactions are dominant are shown. In this diagram, the photoelectric effect take place for low energy photons and with materials which have high number of atomic number Z . The Compton scattering interaction occur for moderate energies. Pair production take place for both high energy and materials with high atomic number Z .

2.3.1. The Photoelectric Effect

Researchers show us that light consists of particles. These are called as photons which carry energy. In the photoelectric effect, the incident photon is absorbed by the

material and the electron is emitted in this process. Emitted electrons are called as photoelectron [20].

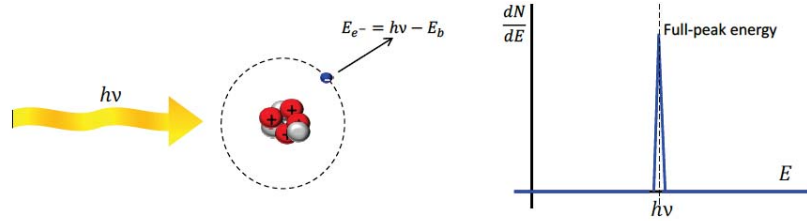


Figure 2.4. Photoelectric effect and histogram [21]

It is clearly visible in Figure 2.4, an incident photon has $E = h\nu$ energy and an electron has binding energy which is shown E_b . The incident photon with energy $h\nu$ interacts with the atom and gets absorbed by the electron. Thus, the electron is released with a kinetic energy which is calculated by subtracting binding energy of electron from photon's energy.

$$E_{e^-} = h\nu - E_b \quad (2.1)$$

In photoelectric interaction, an ionized absorber atom is created with a vacancy in one of its bound shells. This vacancy is will be quickly filled by an electron from a shell with a lower binding energy (other shells) or through the capture of a free electron from the material. The rearrangement of electrons from other shells creates another vacancy, which, in turn, is filled by an electron from an even lower binding energy shell. Therefore, a cascade of more characteristic X-rays can be also generated. The probability of characteristic x-ray emission decreases as the atomic number of the absorber decreases.

In some case in the photoelectric effect, a vacancy in K-shell that is created as a result of photon interaction can be filled by another electron from the M-shell fills this vacancy but releases some energy in the process equal to the difference between two energy level. This photon is shown to have knocked off another electron from the M-shell. The end result is a radiationless electron emission. This electron is called Auger electron.

A single energy's photopeak of incident gamma-rays is shown in Figure 2.4. Photoelectric absorption is dominant when gamma rays have small energies.

2.3.2. The Compton scattering

Compton scattering is observed when the incident photon interacts by free electron or with loosely bound electron in valence shell (outer shell). The photon transfers part of its energy to the target electron, and then both the recoil electron and the photon scatter with a certain angle, while the photon preserve the rest of its energy. The energy of the recoil electron as a function of θ :

$$E_{e^-} = h\nu - h\nu' = h\nu \left(\frac{(h\nu/m_0c^2)(1 - \cos(\theta))}{1 + (h\nu/m_0c^2)(1 - \cos(\theta))} \right) \quad (2.2)$$

As shown in the equation 2.2, the energy of recoil electron depends on the angle of the photon which is scattered.

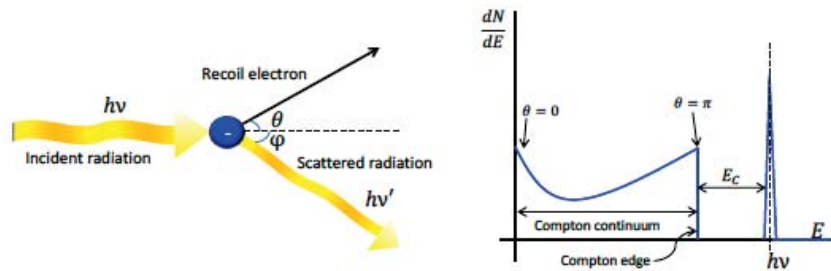


Figure 2.5. Compton scattering [21]

- For $\theta \cong 0$, the incident photon lost so little part of its energy and scatter with almost the same energy. Thereby, the recoil electron moves with little energy.
- For $\theta \cong \pi$, between the incident photon and the target electron, maximum energy transfer takes place.

In a detector, all scattering angles from 0 to π can take place. As can be seen in Figure 2.5, a continuous range of emitted energies is produced by the recoil electron. E_c refers to the gap between the gamma ray and the Compton edge. The Compton effect is dominant for intermediate gamma-ray energies [16].

2.3.3. Pair Production

Pair production is the last significant interaction process. Pair production is a phenomenon of nature where energy is converted to mass. An electron-positron pair created by a photon and interaction must occur in the Coulomb field of the nucleus because of the conservation of momentum, that is, pair production cannot take place in empty space; something must absorb the momentum of the initial photon. The photon momentum can be absorbed by an atomic nucleus, which is thousands of times more massive than an electron or positron and can, therefore, absorb momentum without absorbing much energy; therefore the energy-conservation remains approximately valid. Consequently, pair production is observed when high-energy gamma rays enter a solid. In that case, when the photon has 1.022 MeV energy and above, pair production take place because the resting energy of positron and electron is 511 keV. If the photon's energy is the higher than 1.022 MeV, the surplus is shared between them as kinetic energy. Assume that total energy of the electron and positron is stored in the detector capacity, the stored energy is given by

$$E_{e^-} + E_{e^+} = h\nu - 2m_0c^2 = h\nu - 1.022\text{MeV} \quad (2.3)$$

As can be seen from equation 2.3, to create electron-positron pair , the energy must be $E_\gamma \geq 1,022\text{MeV}$.

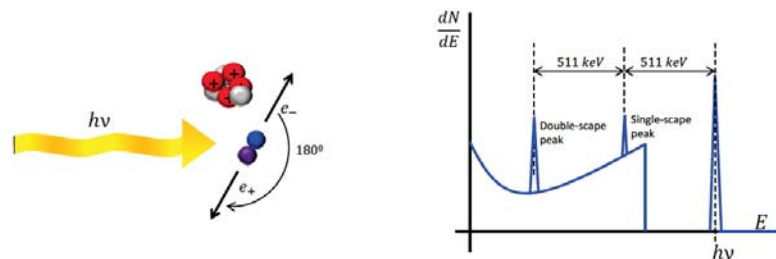


Figure 2.6. Histogram of the pair production and energy distribution [21]

There exists an inverse process to pair production called pair annihilation. Pair Annihilation means the reverse process of pair production. In the pair annihilation, the electron and the positron in the stationary state combine with each other and annihilate.

Surely, the particles are disappeared and radiation energy will occur instead of two particles. For the momentum conservation, the most frequent process in pair annihilation is making two photons that have exactly opposite direction and the same amount of momentum. These two photons have energy 0.511 MeV before losing its energy completely. Gammas created by pair production can escape doing Compton scattering or their energies' can be stored with photoelectric absorption in the detector. Just like photoelectric absorption, to pair production to occur, in other words, to conserve momentum, the event has to take place in an atom. As can be seen from Figure 2.7, This process generates the single and double escape peaks observed in the spectra.

2.4. Detection of Gamma Rays

Nowadays, various methods are used to detect gamma rays. Detection of gamma radiation is one of the most important research tools in nuclear physics. It yields information on various properties (excitation energies, angular moments, decay properties etc.) of states in nuclei. In this section, gamma-ray spectroscopy and gamma-rays that are used at detection methods are introduced. In Figure 2.8, the spectrum that shows three different interactions of single gamma-ray energy is analyzed. In this spectrum, the vertical axis shows counts (number of the event) per channel that detector measured, the horizontal axis shows the stored energy in the detector that corresponds to each channel.

It is a typical gamma spectrum that shows up when the detector interacts with a single energy gamma that sent to detector. In this spectrum, it is named as full energy peak that all of incident gamma rays' energy stored in. In other words, it is simple photoelectric interaction and capture all of the kinetic energy from the photoelectron (E_γ).

The area under this peak gives a number of gammas that stored all energy in the detector volume. These energies of gammas are the value of photopeak energy. When looked at the types of interaction with matter of gamma rays, the results of Compton scattering and pair-production can be seen in the spectrum which are another types of interaction. Compton continuum occurs in the spectrum if all of the gammas escape via Compton scattering without storing all of their energies in the detector. In this area gamma ray energies cannot be determined accurately.

If the incident gamma ray's energy is greater than or equal to 1,022 MeV, it is introduced in the previous section that electron-positron pair occurs. Afterward, the positron and the electron annihilate each other. In this case, two 511 keV photon is formed. If one of the annihilation gamma-rays that have 511 keV energies is captured by the detector and

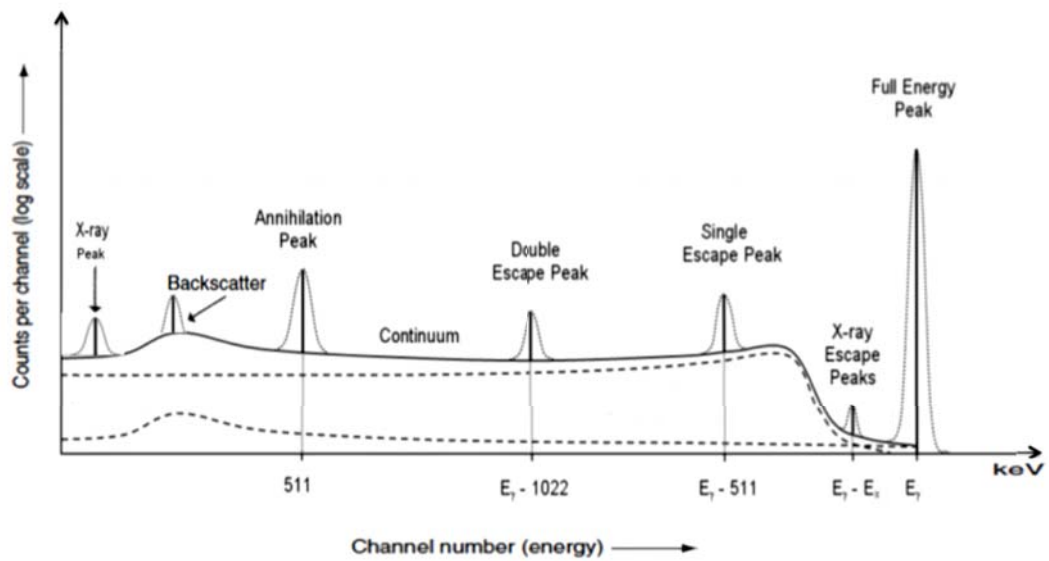


Figure 2.7. Gamma-rays Spectrum [22]

the other gamma, which has 511 keV energy, escape from the detector, it can be seen in the spectrum single escape peak because of escaping one gamma in the detector without interacting. If both annihilation gamma-rays escape this gives rise to the double escape peak.

If a pair production event occurs in the surrounding shielding material, there is possibility that one of the two annihilation photons will deposit energy into the detector. When this happens, an annihilation peak can be observed at 511 keV.

As described in the Section 2.3.1, a characteristic X-ray is released by an absorber atom that is, in most cases, reabsorbed near the atom that emitted it. If this process occurs near the surface of a detector, the characteristic X-ray may escape the detector. Hence, a new peak is created by the characteristic X-ray that escapes. This peak appears a distance of the characteristic X-ray energy away from the full energy peak and is known as the X-ray escape peak. This phenomenon is prevalent in low energy incident photons and detectors with a large surface-to-volume ratio [20].

X-ray peak in the spectrum is a result of the detector absorbing the characteristic X-rays that are emitted from the surrounding materials.

When gamma-ray, before hitting the detector, are scattered at $\theta = 180^\circ$ by Compton scattering in lead shielding and housing, and the scattered gammas are absorbed in

the detector, and then a peak that observed in the spectrum (Figure 2.7) is called the backscatter peak.

2.5. Neutron-Matter Interaction Mechanisms

Due to being neutral, the detection process of the neutron is difficult. As we know, gamma-rays interact with electrons directly in the detector, while neutrons do not [23]. More specifically, the interaction phenomenon occurs between neutrons and nuclei. When a neutron collides with a nucleus, it deviates its path and scatters into a new direction or absorbed. Those processes depend on the energy of neutrons. Many types of neutron interaction with the nucleus are shown in Figure 2.9.

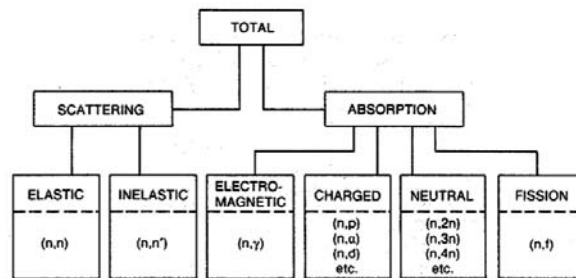


Figure 2.8. Schematic view of neutrons interactions [24]

First of all, analyzing scattering process, when a neutron is scattered by a nucleus, the neutron loses some part of their energy, change direction and lower the speed. On the other hand, proton and neutron numbers remain same in the nucleus. The nucleus gains recoil velocity and it can be left in an excited state, for this reason, it releases radiation.

Scattering events subdivide into elastic $A(n,n)A$ and inelastic scattering $A(n,n')A^*$, where this notation $X(Y, Z)T$ means the interaction Y element with X nucleus, generating afterwards the interaction the nucleus T and the particle Z , mainly produced in the MeV range [24]. In elastic scattering, neutrons lost some part of their energy due to transfer of their kinetic energy to the nucleus, nonetheless, total kinetic energy is unchanged throughout the interaction. In-elastic scattering event refer that after the nucleus collides with the neutron, the nucleus undergoes into an excited state and finally releases radiation. This event occurs when the neutron energy is especially high (> 1 MeV), moreover, the nucleus does not change to an excited level in elastic scattering. However, the total

energy of the neutron and the nucleus after the collision is less than the kinetic energy of the incoming neutron.

Another type of neutron interaction is the neutron capture or absorption. These phenomena generate many possibilities such as rearrange its internal structure or release gamma rays. On the other hand, charged particles can be emitted. As can be seen clearly in Figure 2.9 the most prevalent ones are proton (n,p), deuteron (n,d), alpha particle (n, α) and fission products (n,f) after the neutron capture or absorption event. Neutrons cannot be detected directly because of their uncharged nature. In that case, first of all, the neutron is absorbed by the nucleus and eventually, it emits a charged particle and it is called secondary process. Finally, it can be detected via the secondary process.

Detection of neutrons depend on the energies of neutrons. Therefore, there are many types of the detector such as ionized 3He , BF_3 chambers for slow neutrons [23], while 4He , CH_4 for fast neutrons also neutron interaction with aromatic scintillators NEDA and Neutron Wall respectively.

CHAPTER 3

FUNDAMENTALS OF SEMICONDUCTOR PHYSICS

3.1. Electrical Classification of Solids

Solids are classified with respect to their electrical conductivity; conductors, insulators, and semiconductors. Conductor materials contain many free electrons, for this reason, they can move freely inside materials and they are objected to move with applying little potential. After electrons start to move, they collide with each other and then start the flow of electric charge, which is called the electric current.

Insulator materials do not involve free electrons and those electrons bound to an atom. To break off these bonds, if the electrical potential is applied to conduction materials, this electrical potential must be too high. Furthermore, if the material is not strong as a structural, this high voltage can broke the material structure.

Semiconductor materials are between conductors and insulators with regard to electrical conductivity. In other words, electrons are neither almost entire free nor bound to the atom in the material. Electrons cannot move at low temperatures under any voltage. If one is increased the temperature of a semiconductor, electrons may move and electric current will flow at moderate voltages.

The band gap is an important property of solids, conductors, insulators, and semiconductors that can be classified. In atoms and molecules, electrons just can be allowed energy levels, which is called band. In other words, the energy levels consist of energy bands. The energy levels are occupied by electrons, which start with the lowest energy level. Electrons can only exist allowed energy bands. Energy band gap E_g is shown as an alteration with respect to materials (Figure 3.1).

Electrical conduction depends on the contribution of the electrons that are occupied an energy band. The electrons that are located in the outermost shell are called valence electrons and the valence electrons responsible for the chemical properties of an atom. The highest energy band that occupied electrons is called the valence band. In the insulator, valance band is exactly occupied. The next allowed band that has unoccupied states is called the conduction band and it is completely empty in insulators. Since the

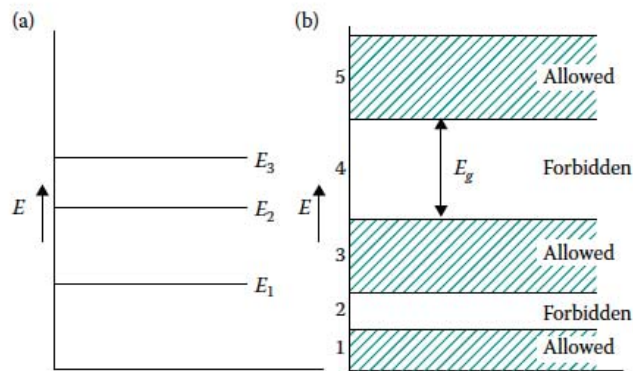


Figure 3.1. (a) The atomic energy levels are discrete lines. (b) In a solid, the allowed energy states become energy bands [19]

energy gap is extensive, the tally of occupied states is always zero in the conduction band (Figure 3.2). To provide the conductivity, electrons have to cross from the valence band to the conduction band, which means that the band gap represents the minimum energy that is required to excite an electron up to the conduction band. However, electrons cannot be found in the conduction band and they cannot generate an electric current under an electric field.

In conductors, the valance band lap over with conduction band (Figure 3.2). Thus, most of the electrons in the valence band can jump to the conduction band without applying external energy.

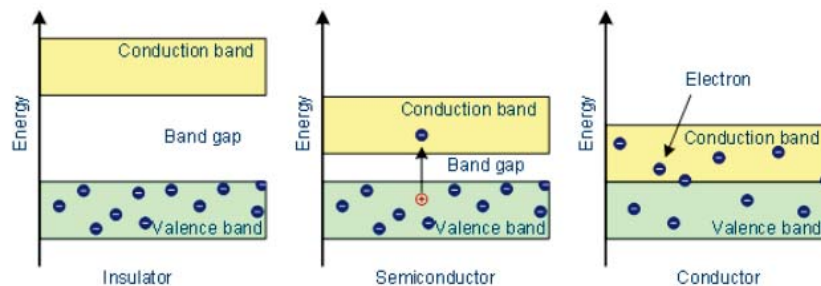


Figure 3.2. Band structure of solids [25]

Semiconductors that have a narrower band gap between the valence band and the conduction band are neither exactly good conductor nor exactly good insulator. At

absolute 0 temperature, in a pure semiconductor the valence band is completely filled and the conduction band is vacant. When a small amount of energy is supplied, the electrons can easily jump the forbidden gap, thus allowing electrical conduction. The absence of an electron in the valence band is referred to as a hole. This process called electron-hole pair generation. That hole is treated as particles with the positive charge. Moreover, when the electrons move in a direction with an electric field, the holes move opposite direction because of its charge, that is, it responds to the force applied to them by the field. The electrons in the valence band can move thanks to the holes.

3.2. Extrinsic and Intrinsic Semiconductors

The semiconductor is divided into two types; Intrinsic or pure semiconductor and extrinsic or impure semiconductor.

An intensely pure semiconductor is called as Intrinsic Semiconductor. Silicon and Germanium are categorised as intrinsic semiconductors, that is they are chemically pure, including nothing but semi-conductive material. In intrinsic semiconductors such as germanium or silicon, the conduction band is empty and valence band is completely filled up with electrons at very low temperature. Due to the fact that germanium and silicon have four valence electrons, each atom of them shares one electron with its adjacent atom. That process is called the covalent bond. Intrinsic semiconductors do not contain free electron. Therefore there is no conduction of electricity in them. As we mentioned in the previously section, when an electric field is applied, electrons jump the conduction band and they leave behind the holes in the valence band. For this reason, the number of electrons in the conduction band and the number of holes in the valence band is equal each other. And so, the overall electric charge of an atom is neutral.

An extrinsic semiconductor is an impure semiconductor, which means that when the impurity is mixed in the intrinsic semiconductor, the conductivity of semiconductor goes up. And also it is known as doping. There are two types of extrinsic semiconductors with respect to the added impurity.

3.2.1. n-type Semiconductors

The n-type semiconductors are obtained when Group-V elements which are phosphorous, arsenic or antimony are added into intrinsic semiconductors. As we know, there

are five electrons in the last orbital of the arsenic atom, which means that the arsenic atom can make 5 bonds, however, the outer orbital of the silicon has 4 electrons and the silicon makes 4 bonds. If the arsenic atom is doped into the silicon crystal atoms, the arsenic makes the covalent bond with the 4 electrons of silicon in the outer orbital, but the fifth electron of the arsenic finds no place in the covalent bond. Then it joins to electrical conductivity, so conductivity increases. The atoms give extra electrons to the material in this way called donor atoms.

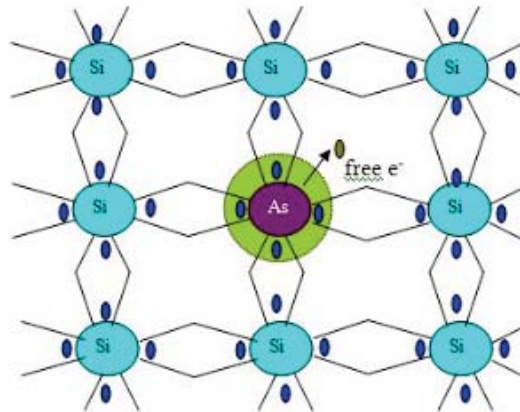


Figure 3.3. n-type semiconductor [26]

Electrons generally called as carrier current in the n-type semiconductor. Although several electron-hole pairs are taken place with thermal energy in n-type semiconductor, that holes cannot be generated with the addition of the dopant. Holes are called as minority charge carriers in the n-type semiconductors.

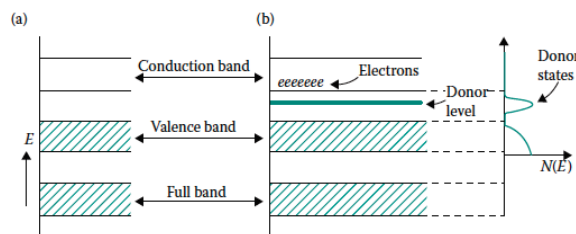


Figure 3.4. (a) Intrinsic and (b) n-type semiconductor. New electron states (donor states) are created close to the conduction band [19]

The N-type semiconductor has a large number of electrons. This does not mean that electric charge of the n-type semiconductor is negative. Despite the fact that it contains many mobile electrons that are provided by the donor atoms, the total electric charge of the n-type semiconductor is neutral.

3.2.2. p-Type Semiconductors

The p-type semiconductors are obtained when Group-III elements such as gallium, indium or boron etc. are added into intrinsic semiconductors. All these atoms have three valence electrons, therefore, if the silicon (or indium or boron, does not matter) is doped with the gallium, just three valence electrons of silicon make the covalent bond with three valence electrons of the gallium. As we know, silicon has four valence electrons, which mean that one valence electron of silicon cannot make covalent bond, for this reason, one hole is generated for each gallium atom. The dopant is negatively charged because the gallium atom behave negative ion when it accepts the extra electron, such dopant atoms are called acceptor atoms.

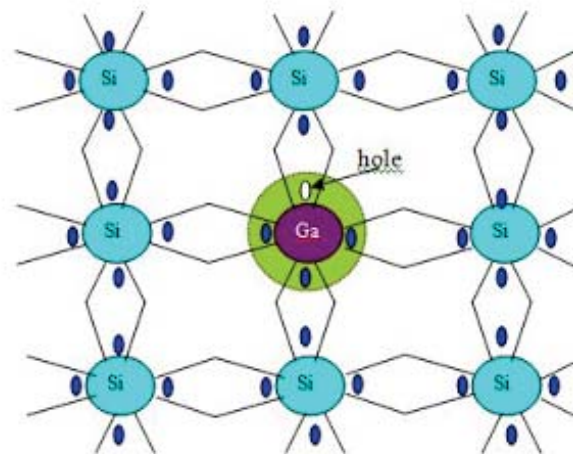


Figure 3.5. p-type semiconductor [27]

By virtue of thermal energy, hole-electron pairs are generated. However, the number of holes are too high compared to the number of electrons and electric charge of p-type semiconductor is neutral, even if it contains many holes that are provided by acceptor atoms. Holes called as carrier current in the p-type semiconductor. In brief, in a

p-type semiconductor, holes are majority carriers and electrons are minority carriers and in an n-type semiconductor electrons are majority carriers and holes are minority carriers.

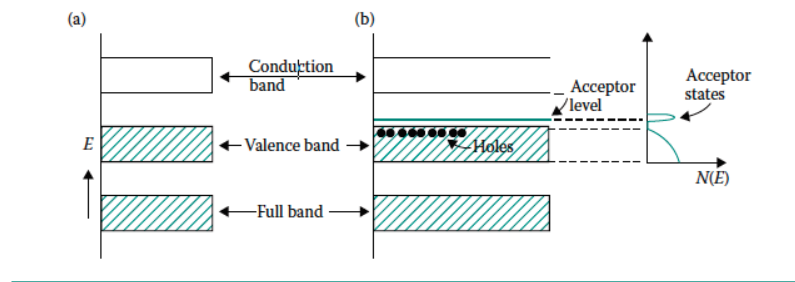


Figure 3.6. (a) Intrinsic and (b) p-type semiconductor. New hole states (acceptor states) are created close to the top of the valence band [19]

3.3. The p-n Junction

Semiconductors are the most important materials for radiation detection since they are useful for their controllability not for their conductivity. This controllability and conductivity have been used in microchips, transistors as well as detector systems.

P-n junctions are formed by combining n-type and p-type semiconductor materials. There are many free electrons on the n-type zone side, on the other hand, there are many holes on the p-type zone side (Figure 3.7). Both sides have high concentration electrons or holes. When this two type of semiconductors is joined, electrons get repelled from each other because of the high concentration of electrons at n-type side. And then, electrons diffuse from the n-type zone to the p-type zone. Likewise, holes diffuse from the p-type side to the n-type side. This diffusion process will be continued until equilibrium is reached. The encounter of holes and electrons eliminate each other. While the absence of electrons creates positive ions in the n-type zone, the absence of holes creates negative ion in the p-type zone.

There are no mobile charge carriers near the p-n junction region. This region called depletion region. Depletion region acts like a barrier that goes against the flow of electrons from the n-type zone and holes from the p-type zone. To exceed this barrier, the external voltage should be applied which is greater than this barrier potential. Thus, electric current starts following. As a result of accumulative charge in the depletion region,

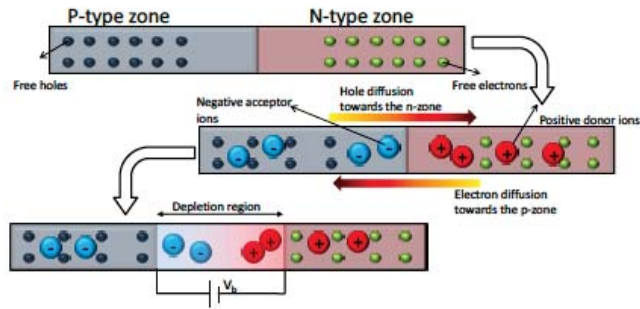


Figure 3.7. Creation of the depletion region in a p-n junction [21]

this process signals a non-zero local electric field contact potential V_b , which is usually 0.3 V for Ge and 0.7 V for Si.

If the positive station of a voltage resource is applied to the n-type contact and negative station of a voltage resource is applied to the p-type contact, this process is called reverse bias. In this case, electrons in n-type side move toward the positive terminal while holes in p-type side move toward the negative terminal and an electric field extends across this sensitive region.

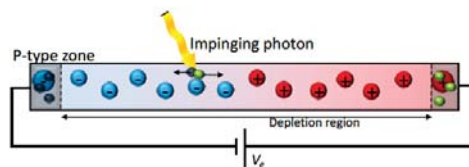


Figure 3.8. Radiation detection mechanism in a reverse-biased semiconductor [21]

3.4. The High Purity Germanium (HPGe) Radiation Detectors

The nuclear structure has been explored by using Ge detector. HPGe (High-purity Germanium) became important for High-resolution gamma spectroscopy in the late 1970s. Ge detectors were developed for volume and purity among 1970s and 1980s

[28–30]. Lately, the improvement of highly- segmented Ge detectors have extremely increased the efficiency and the energy resolution.

High energy resolution detectors should be used to distinguish two gamma-rays which have close energies. Since HPGe detectors have high energy resolution, it is a perfect choice for this type of circumstances.

A HPGe is a diode which is produced by highly pure Ge crystal. It can be produced by p-type material or n-type material. Moreover, it allows a variety of contacts to be used. Nowadays, net impurity concentration of p-type and n-type crystals are 10^{10} atoms cm^{-3} . Therefore, some of the most important properties of HPGe detector are low impurity concentration, high resolution, and large depletion region, which is a necessity in order to produce an electron-hole pair with low ionizing energy. Whereas n^+ hole-blocking contact is produced by lithium diffused into the crystal, p^+ electron-blocking contact is produced by boron implication into the crystal. HP-Ge detectors are produced primarily two types of configurations which are planar configuration and coaxial configuration, respectively. (Figure 3.8)

Planar HPGe detector has two flat surfaces and so electrical contact ensure thanks to this surfaces. As mentioned in the previous section, if a positive electrode is applied to the n^+ contact and a negative electrode is applied to the p^+ contact a reverse bias occurs. Thus, the width of the depletion region increases. Consequently, HPGe detector becomes fully depleted.

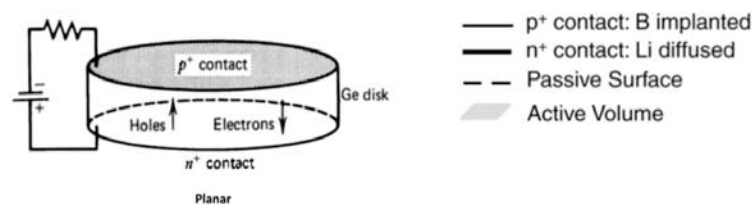


Figure 3.9. Configuration of Planar [31]

A planar HPGe n-type detector is produced in following way, the n^+ contact is placed at the right side of the n-type crystal, p^+ contact is placed at the left side of the n-type crystal. To produce p-type HPGe detector, n^+ contact is at the left side of the n-type crystal, p^+ contact is at the right side of the n-type crystal. And then when a reverse bias is applied the whole n-type crystal or the whole p-type crystal, depletion region will be occurred.

A fully depleted detector is very important to obtain a pulse because when incident gamma rays interact with depletion region, electrons are excited by gamma rays and they move toward the conduction band. Thus, electron-hole pairs are generated. These electron-hole pairs instantly drifted toward each electrode by the electric field. Therefore, charge-sensitive preamplifier converts these charges into the voltage pulses proportional to the energy deposited in the detector.

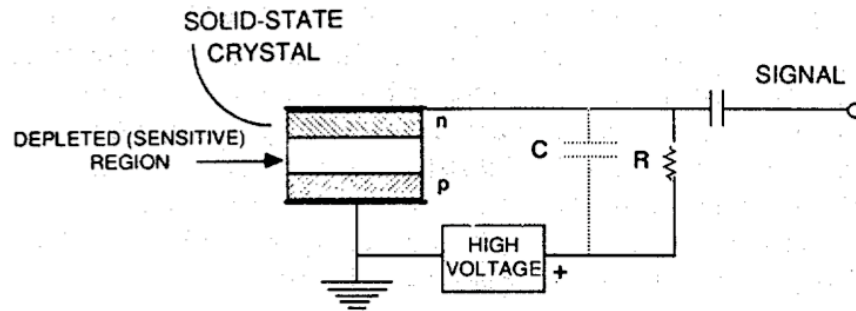


Figure 3.10. Typical arrangement of components in a solid-state detector [32]

Planar detectors are not relatively convenient to produce large volume germanium detectors. In that case, coaxial or cylindrical geometry ensure more advantages to large detection efficiencies at high gamma rays. Coaxial detectors are produced in order to increase depletion region. Many configurations of coaxial germanium detectors are produced such as true coaxial and closed-ended coaxial as can be seen in Figure 3.11. Also, they have fabricated both HPGe n-type coaxial detector and HPGe p-type coaxial detector. For p-type coaxial, n^+ contact is located at the outer cylindrical surface and p^+ contact is located over the inner cylindrical surface. The contacts of HPGe n-type coaxial detector is located opposite way with respect to the p-type coaxial HPGe detector. In p-type coaxial detectors, outer contact which is Li-diffused has frequently 0.5 mm thickness, whereas, in n-type coaxial detectors, outer contact which is boron implanted has 0.3μ thickness [33]. The thin entrance window takes advantage for spectroscopy of low energy of gamma rays that is why n-type detectors are preferred. There is one more important reason to choose n-type detectors that is radiation damage. Since HPGe detectors have high resolution, they are sensitive to radiation damage. Nevertheless, low sensitivity of n-type detectors to radiation damage is caused by neutrons [34, 35]. Fast neutrons are emitted in any nuclear reaction with beam energies above the Coulomb barrier. These fast neutrons which

have sufficient energies can dislocate the Germanium atoms in detector crystal. These dislocations lead to defects. These affects the performance and resolution of detector because the dislocations can act as traps for holes, electrons, moreover, they may create new donor or acceptor levels. These levels can capture electrons or holes and they release them after a period of time. Clearly, if the trapping time is long, the captured carriers cannot contribute to the measured pulse. All these phenomena change both the charge collection and so the energy resolution. However, the novel n-type HPGe are clearly less precise to neutron damage [34].The effects of radiation damage can be reversed with an annealing process. It is necessary to just heat the detector crystal up to to 250° and for the period of almost 1h and re-etching [30].

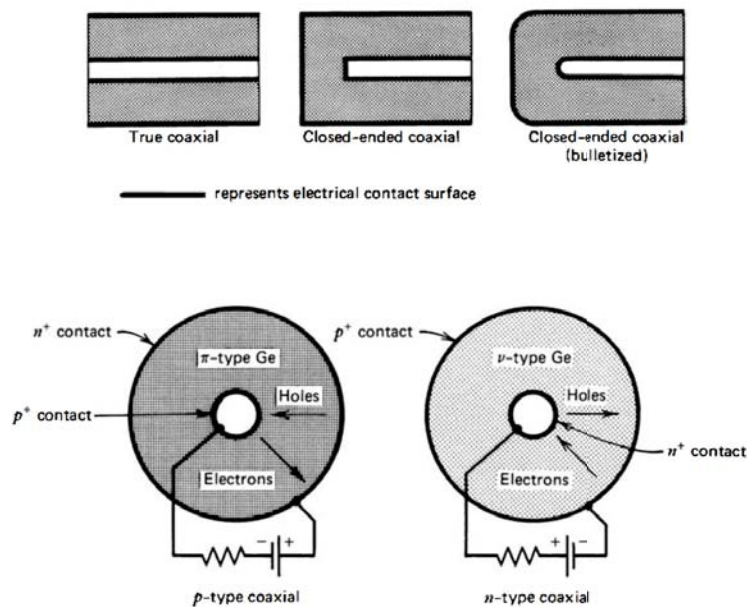


Figure 3.11. Three common shapes of coaxial detectors. At the bottom shows n-type and p-type geometry and cross section of coaxial detectors [31]

Owing to the fact that Germanium has the relatively small band gap (0.7 eV) at room temperature, germanium detectors must always be cooled by liquid nitrogen that has a temperature of 77 K, which decreases thermally generated leakage current, when in use. Furthermore, a leakage current thermally generates electrical noise in the crystal, that is, cooling the detectors is important in order to reduce the contribution of noise associated with leakage current.

3.5. Energy Resolution

The aim of many concepts of radiation detectors is to measure energy distribution. Radiation detectors should have better capability to distinguish between radiations of similar energy, which is called energy resolution. Good energy resolution depends on the type of detector as well as the electronics because energy spectrum is obtained by the noise of the readout electronics. Energy resolution is generally determined using a term which is called Full Width at Half Maximum (FWHM). The FWHM is described as the width of the distribution at a level that is just half the maximum ordinate of the peak. Nowadays, there are many applications or software to measure FWHM.

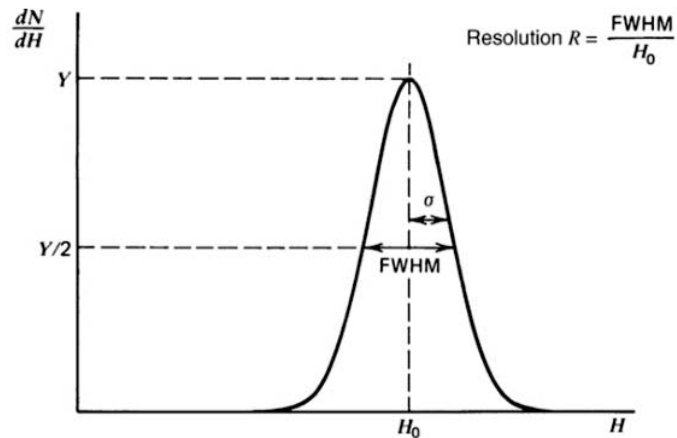


Figure 3.12. Response function of the detector in Gaussian shape [31]

For pulse or peak shape in Figure 3.12 gives the definition of the energy resolution (FWHM). FWHM is given by $FWHM=2.35\sigma$, where σ is the standard deviation of Gaussian shape. The lower the FWHM value, the greater the sensitivity level of the detector and the two closely related gamma energies will be able to distinguish. The energy resolution R is thus a dimensionless term always expressed as a percentage. H_0 in Figure 3.12 is the mean energy value of the peak.

CHAPTER 4

THE EXOGAM DETECTOR AND THE NUMEXO2 DIGITIZER

4.1. EXOGAM Detector and Array Design

EXOGAM (EXOTic GAMma array spectrometer) has been used with cooperation an array of high-purity Ge detectors by using the exotic radioactive beams from the SPI- RAL (Système de Production d'Accélération en Ligne) accelerator. At the present time it is located at GANIL (Grand Accélérateur National D'Ions Lourds), in Caen, France.

Since gamma-ray spectroscopy detectors have been improved recently, these make it possible to research of nuclei that are undiscovered regions of the nuclear chart or regions of far from the stability. One of the most significant properties of High-resolution spectrometers is that these are sensitive to detection of the weak transitions in the gamma spectra. Thus, the main purpose of the design of EXOGAM was the optimization of the photo- peak efficiency, in other words, to maximize the total photo-peak efficiency, while conserving the quality of spectra. Another important properties is that Compton scattering leads to noise into the signal because a wide range of electron energies can come from a single ray, therefore, an optimized signal-to-noise ratio and especially high resolution within energy and time are important with respect to spectrum quality. In exotic beams experiments, it is a very challenging process to get high signal-to-noise ratio and a good resolving power [35]. Moreover, because of the major radiation environment in experiments, radiation shielding and geometrical design become considerably crucial. Different array design can lead to need for different experimental conditions; therefore, EXOGAM allows combining with ancillary detectors with respect to the type of experiment. Ancillary detectors also are of vital importance to detect both light and heavy charged particles and neutrons. The SPIRAL facilities enable to produce exotic ion beams and high-intensity stable ion beams. That gives an opportunity to physicists to investigate nuclear structure deeply [36].

4.1.1. EXOGAM Design Specification

EXOGAM is composed of an array of high-resolution germanium detectors that located close to the target point. These have been organized to give a high photo-peak efficiency 20 % at 1.3 MeV gamma rays [38]. Each germanium detectors are enclosed by an escape suppression shield generally performed from bismuth germanate (BGO). Thus, suppression shield develops the spectrum quality. High- purity germanium detectors which created EXOGAM are coaxial n-type HPGe crystals. Additionally, each one of the four germanium crystals constitutes the segmented CLOVER detector that is placed in the same cryostat.

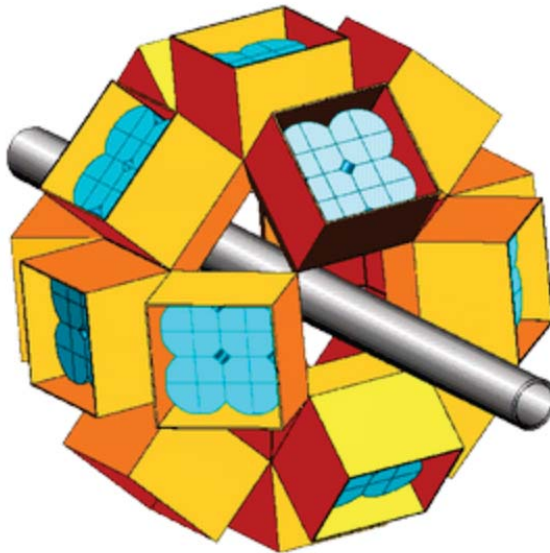


Figure 4.1. EXOGAM detector array design [4]

EXOGAM is constituted by using 16 large volume HPGe segmented Clover detectors in closed packed configuration (Figure 4.1). Segmentation design plays a major role in order to decrease the Doppler broadening and multiple-hits incidents. Doppler broadening can be observed in gamma-ray spectroscopy and it leads to the peaks in the spectra to broaden because of the distribution of velocities by the Doppler effect. In this way, each individual crystal in the segmented Clover detectors minimise the effect of Doppler broadening and it is necessary in order to maintain good energy resolution [38].

4.1.2. Segmented CLOVER Ge detector

The EXOGAM array design is composed of segmented CLOVER detectors. Each Germanium crystal that is located in the same cryostat have been electronically segmented into four regions (Figure 4.2). This segmentation is a significant requirement, not just because to get large volume but also to determine impact point of gamma-ray in the detector better. Moreover, segmentation design gives rise to reduce Doppler broadening because of the closed packed and efficient design. Especially, a nucleus that emitted gamma-rays has high recoil velocity for this reason segmentation that is suited close geometry is effective for those gamma rays which is scattered with a broad range of scattering angles.

High granularity is an obligation in order to maintain the good resolution and correct the gamma ray peaks for Doppler broadening [38]. Granularity is therefore obtained by segmentation.

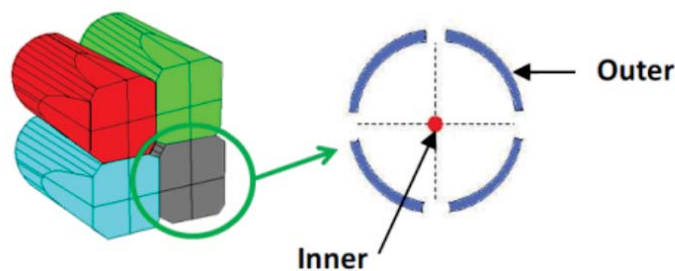


Figure 4.2. Left: A schematic diagram of the crystals in a segmented CLOVER Ge detector. Right: Zoomed segmented crystal [4]

As can be seen clearly from the right side in Figure 4.2, each crystal that is in Clover detector has an inner contact and four outer contacts, located at the corners of each crystal and these allow the position of the event to be specified. High energy resolution signals are output from inner contacts (2.1 keV at 1.3 MeV) due to cooled pre-amplifier stage close to the contact whereas lower resolution signals are output from 16 outer contacts.

Each germanium crystal made of 60 mm in diameter and 90 mm long. The rise diameter enables the best performance with a compact design and the solid angle coverage

of germanium. Each segmented Clover Germanium detector is surrounded by an escape suppression shield such as a layer of scintillators like BGO or CsI(Na). Those are called anti-Compton shield. When Compton scattering happens inside the germanium crystals by gamma rays, they escape from active volume this means that only a portion of their energy is transmitted to the detector. Furthermore, the pulse does not contribute to the main photo-peak but appear at a lower energy as part of the background [39]. Compton suppression crystals absorb the scattered gamma rays.

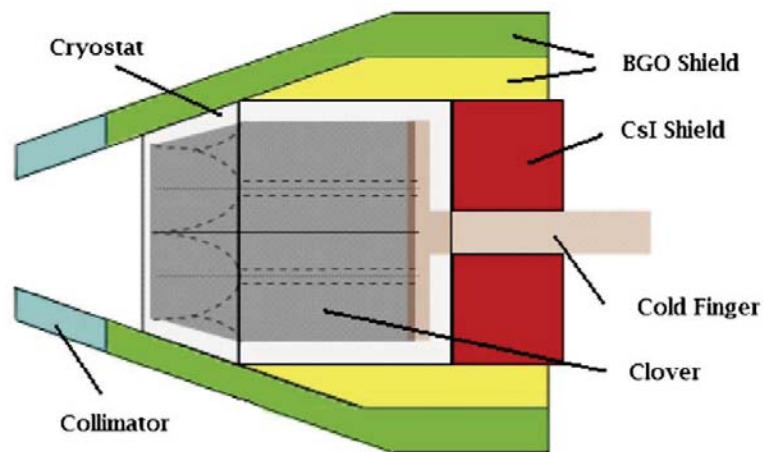


Figure 4.3. The EXOGAM Clover inside its BGO escape suppression shield, consisting of a rear shield to be used in the most compact geometry and an additional side shield to be used for improving the peak-to-total ratio in the pulled-back geometry [4]

As provided by Figure 4.3 The EXOGAM shield is formed from three regions which are a back catcher, a rear side shield, and a side shield. Those have 4 BGO channels for each Clover. When the thickness of the rear side shield is 2.5 cm and width 2cm, simulation demonstrates that almost 95 % of the maximum possible peak-to-total value can be obtained at 1.33 MeV [4]. The thickness of the backscatter which composed of CsI(Na) is 4 cm and it gives same performance at lower cost, relatively. Additionally, those have 4 CsI(Na) channels for each Clover. In total, each segmented composed Clover detectors include a set of 28 contacts, which consist of 20 for HPGe channels, 4 for BGO channels, and 4 for CsI(Na) channels.

As we mentioned in the pervious section, EXOGAM array consist of 16 segmented CLOVER detectors and these are located with 4 detectors at 135° , 8 detectors at 90° and 4 detectors at 45° to the beam direction. A cross-section schematic representation

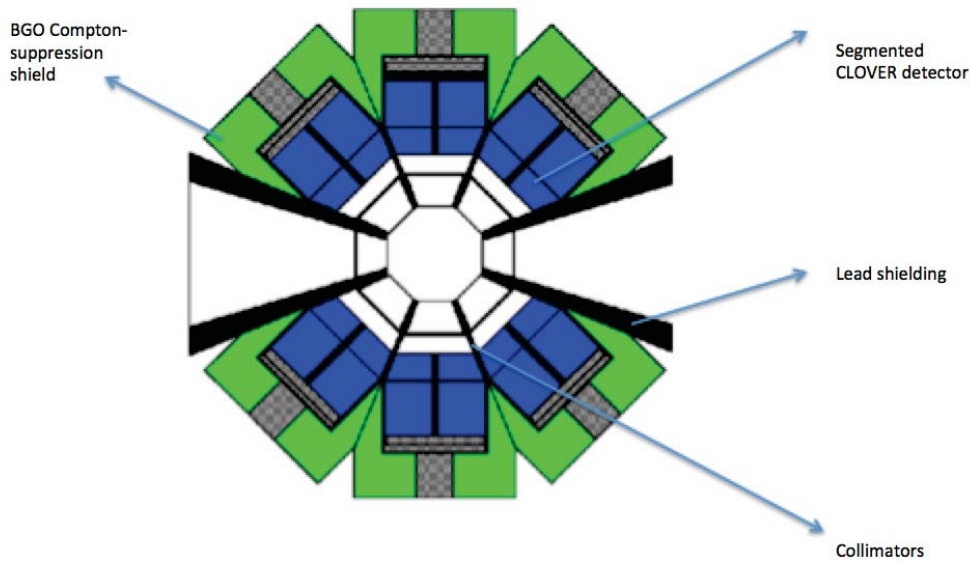


Figure 4.4. A Cross-section through the 16 segmented CLOVER EXOGAM array [4]

of 16 segmented CLOVER EXOGAM array is shown in Figure 4.4. As we mentioned about CLOVERs design, configuration shows an alteration from experiment to experiment. Ge crystal to target distance is $d=11,4$ cm in segmented CLOVER array, which is called configuration A, whereas Ge crystal to target distance is $d=14,7$ cm in segmented CLOVER array, which is called configuration B. Figure 4.4 shows a cross-section through 16 segmented CLOVER geometry in configuration A. This design allows space for beam in and out.

4.1.3. EXOGAM2 Electronics

Segmented HPGe detectors are used in EXOGAM in order to obtain good energy resolution and spectrum quality. Signals that come from the detector should be analyzed in a good way in order to benefit from that segmentation design efficiency. For this reason, a digital electronic system is used instead of an analog electronic system thus, a new digital electronic system is produced for EXOGAM and new EXOGAM is called EXOGAM2. Furthermore, gamma spectroscopy of exotic nuclei and getting more information become possible with the digital electronic system that developed for EXOGAM.

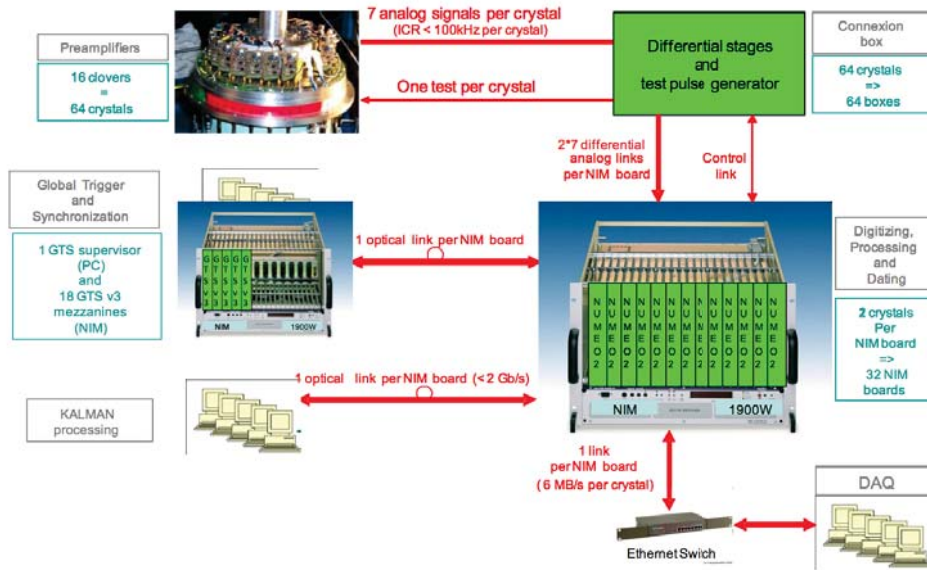


Figure 4.5. Digital electronic system design for EXOGAM2 [40]

In Figure 4.5 shows EXOGAM2 electronics layout. EXOGAM2 electronics upgrade was necessary to have higher counting rates due to taking place interaction phenomena very quickly. Since each event is very important in experiments, data record and control is carried out with ADONIS, which is used to analyze raw data within the digital electronic system in the EXOGAM2 detector. One of the most important reason to use ADONIS technique is to study on the fastest data acquisition performance as possible with new electronic system by adding EXOGAM2 to current EXOGAM.

EXOGAM former readout was based on VXI (VME eXtension for Instrumentation) bus. It supplied larger card options for higher performance, also it allows to define all signals on the backplane. Although VXI had timing, shaping and ADC (Analog Digital Converter) for outer and inner contacts, EXOGAM array needed much more because of their design. As we know EXOGAM consists of the segmented array built, so add-back technique, which is used for the signals from different crystals of clover properly, gained importance. EXOGAM former electronics details can be found in [40].

In order to increase EXOGAM performance, VXI system is altered with fully digital electronics which is called NUMEXO2 (NUMérisieur pour EXOgam2) [41]. The NUMEXO2 digitizer cope with the analog to digital conversion. Moreover, it processes the analog channels and the data readout. Each crystal has 4 outer channels, 1 BGO channel, 1 CsI channel and 2 inner channels contacts. High- resolution energy is obtained by inner

contact. The Global Trigger and Synchronization (GTS) system supplies NUMEXO2 the clock reference, the absolute time and the event trigger phenomenon. The Data Acquisition system DAQ is built with Ethernet network and NARVAL software which provide to running the setup and the readout of the digitizers and the Global Trigger System GTS. The timing of each data, trigger time can be easily controlled by using Global Trigger System. The KALMAN processing system receives raw data from inner channels. KALMAN filter provides both best estimate from noisy data amounts to filtering-out and cleans up the data measurements even onto the state estimate.

4.2. The NUMEXO2 Digitizer

Research on the nuclear structure of exotic nuclei become obligatory to use high-resolution gamma spectrometers in order to pursue the aims the new physics demands. Ancillary detectors are necessary such as neutron and charged particle detectors to determine products from the nuclear reaction. Moreover, electronic systems of detectors play a major role to improve the quality of the data in experiments. Some requirements are a necessity to examine data deeply, some of those requirements are data processing capability, high counting rates, high-speed processing, fast communication as well as energy and timing calculations. Novel technologic array designs have the higher amount of channels besides complex processing algorithms. In that case, analog electronics could not cope with challenge events. At that point, high-speed analog-to-digital (A/D) devices, fast communication optical links and reconfigurable logic devices are used in the front-end electronics [42]. The A/D conversion is fulfilled by Flash Analog Digital Converter (FADC) Mezzanines, part of the NUMEXO2 digitizer.

NUMEXO2 is the core of the NEDA and the EXOGAM2 front-end electronics. The NUMEXO2 digitizer has been developed cooperation with GANIL. The NUMEXO2 digitizer application is set up to be used NEDA (Neutron Detector Array) and EXOGAM2. NEDA is based on excellent neutron-gamma discrimination (NGD) performance and it has efficient detection of neutrons in the energy range from 1 MeV to about 20 MeV [43].

4.2.1. Definition and Block Diagram of the NUMEXO2 Digitizer

NUMEXO2 plays a major role digitizing and pre-processing for NEDA and EXOGAM2. It has many advantageous applications such as A/D conversion, data pre-

processing connection with the Global Trigger System (GTS), as well as communication link management for 16 channels. Moreover, NUMEXO2 power can reach up to 2000W to deliver the rest of electronics in the digitizer. NUMEXO2 digital electronic has data transfer rate 100~200 MHz ($10^8 \sim 2.10^8 Hz$), also NUMEXO2 has capability of to take 14 bits data at 200 Msps (Megasamples per second). It contains 2 high-performance Field-Programmable Gate Arrays (FPGAs), those are the Virtex-6 and the Virtex-5. Figure 4.6 shows the block diagram of the NUMEXO2 digitizer.

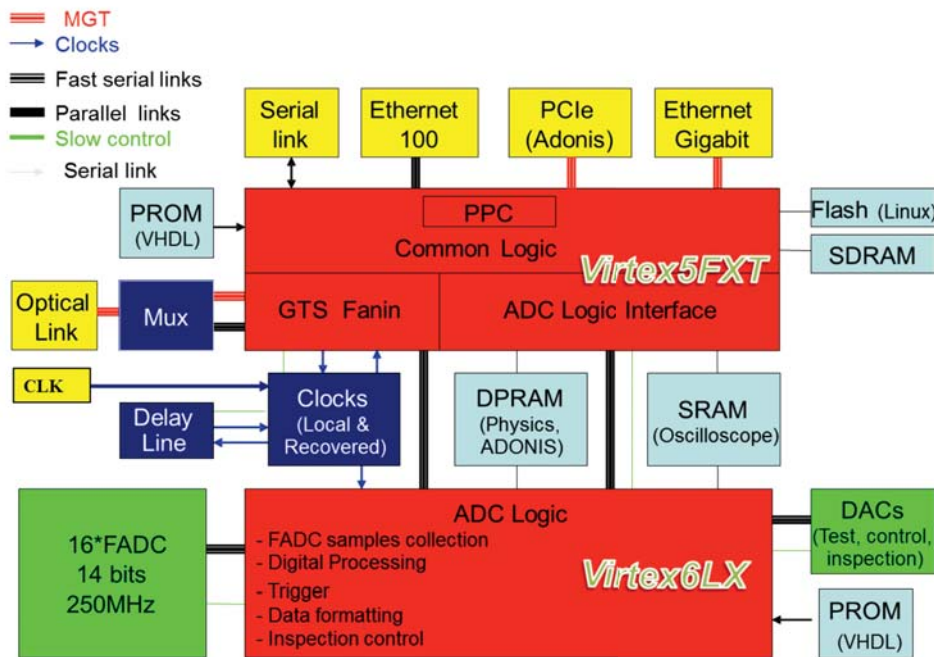


Figure 4.6. NUMEXO2 block diagram [41]

4.2.2. The Virtex-6 Block

The Virtex-6 is one of the logical devices in NUMEXO2. Looking at the characteristics of the Virtex-6, it consists of the oscilloscope, data readout, digital signal processing, setup, inspection lines and FADC data collection (IOSERDES) (Figure 4.7).

- I/O SERDES (Input/Output Serialization-deserialization) block

This block gathers raw data from 4 FADC Mezzanines at 200 MHz sampling frequency. And then, it allocates during 7 differential pairs for each channel and reallocates

it to the rest of the FPGA as samples to be processed by standard algorithms after the deserialization process.

- Digital Signal Processing Board

It can be shown an alteration between EXOGAM2 and NEDA. This block is worked for energy calculation by making use of several blocks. First of all, average Moving Window De-convolution (MWD) carries out a trapezoidal filtering over the original digitized pulse. Following, the energy is calculated as the height between the average of the top and pre-trigger baseline samples. After all, some programs which create histogram organize the energy calculations in a spectral form.

- Oscilloscope

The signals at different points inside the FPGA can be observed by using the oscilloscope. For instance, it can observe raw data from the FADC, as well as data after trapezoidal filtering.

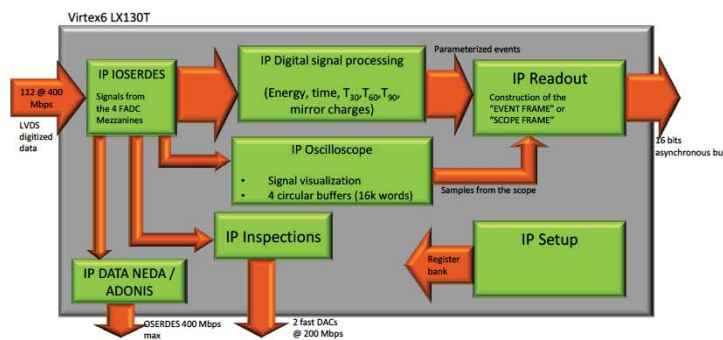


Figure 4.7. NUMEXO2 Virtex-6 block diagram [41]

- Data readout

This block performs the data transmission from the Virtex-6 to the Virtex-5. It contains two different modes such as energy value, timing measurements (parametric mode) and the oscilloscope mode.

- Inspection lines

The IP (internet protocol) consist of the multiplexers and these multiplexers provide to select internal signals at different points of the Virtex-6. Furthermore, they allow driving the signals out of the FPGA so that they can be computed by using the oscilloscope, increasing the test capabilities of NUMEXO2.

- Setup

This block involves registers chains to configure the rest of the blocks in Virtex-6. Registers can read and write thanks to the software tool Ganil Electronic COntrol (GECO) [44] by way of Virtex-5.

4.2.3. The Virtex-5 Block

The Virtex-5 block is the second big-sized device on NUMEXO2 board. The Virtex-5 consist of PCI Express, optical links, serial links and communication drivers, such as Ethernet gigabit. FPGA controls GTS, and GTS synchronize the event that comes from different detectors. Connection to the FADC Mezzanines for each motherboard: 4 Mezzanines will be plugged in it and each Mezzanine can process up to 4 channels. Therefore, each motherboard can collect data from 16 channels. The Virtex-5 block conducts the data that received with from the Virtex-6 after the processing, and the communication ports. Figure 4.8 shows NUMEXO2 Virtex-5 internal block diagram.

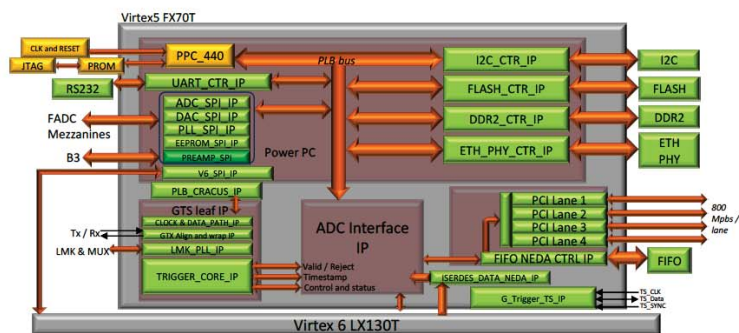


Figure 4.8. NUMEXO2 Virtex-5 block diagram [41]

4.2.4. Data Readout

A software, which is called GRU (Ganil Root Utilities), has been developed by employees of data processing centre of GANIL. This software has the ROOT [45] package program, which is necessary to save and readout the data, and the graphic interface, that based on the programming language C++, which provides convenience to use computer library that is required for analyzing the nuclear physics data. This program is

specially designed for experimental data performed in GANIL, however, it also provides conversion to the ROOT format by using the ROOT package program that commonly used in international research centres. This allows the data to be easily read and made process on, Apart from GRU, the program called VIGRU (Visualize GANIL ROOT Utilities) [46] that visualises the experimental data in GANIL, has been developed, which based on working and processing logic of the ROOT package program. The ROOT can read and measure the data that has the suitable properties in the form of spectrum, matrix, and histogram.

Furthermore, another software has been developed in GANIL, which is called GECO (Ganil Electronic Control). GECO provides control of the NUMEXO2 digitizer units during the experiment and allows NUMEXO2 to run in coordination with another detector systems. Also, GECO enables the required changes on the NUMEXO2 digitizer without entering the test environment.

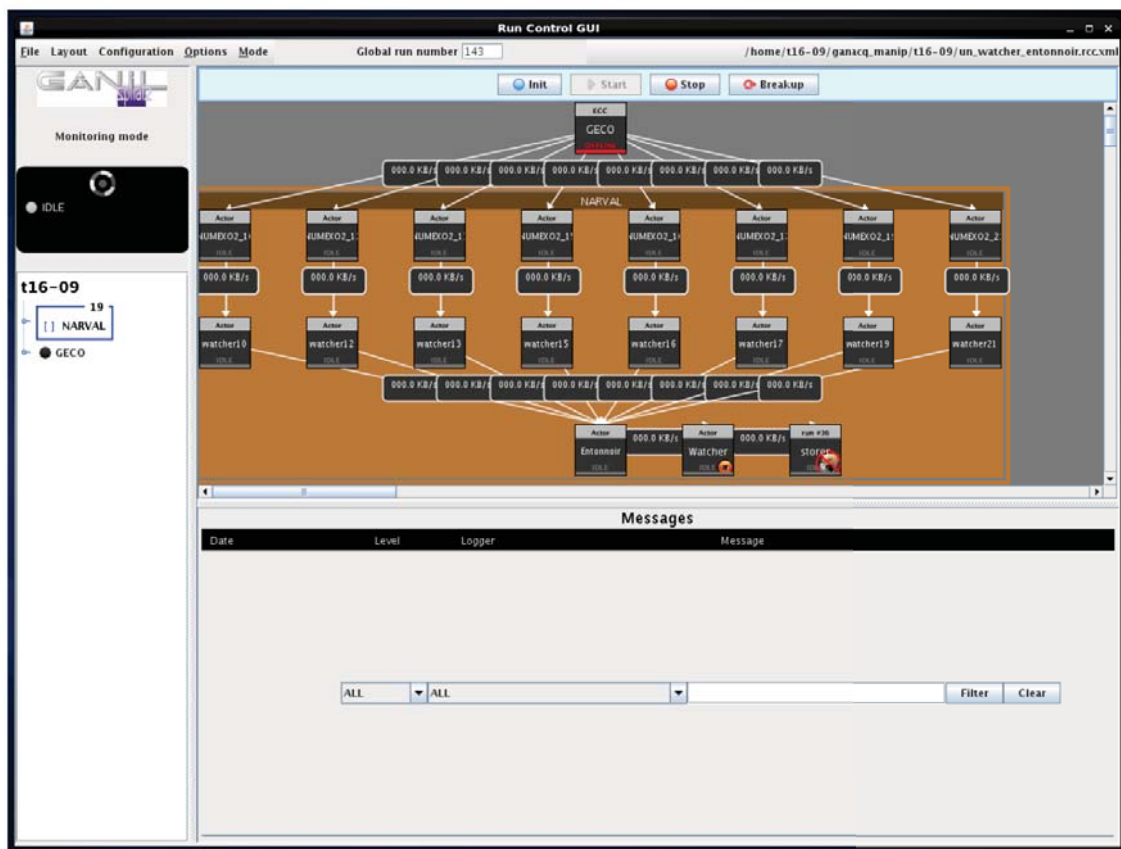


Figure 4.9. GECO test and control interface [47]

Figure 4.9 shows where GECO is placed within test and control interface. As can

be seen in Figure 4.9, GECO and all the NUMEXO2 units that connected to the experimental apparatus and their watcher panel, which the units can be modified or observed is shown. In this control panel, it is possible to see the process of starting and stopping the experiment, at what rate the electronic unit records data and at what rate data record is being made to the storage unit. As can be seen in the flow chart, GECO is important to know what can be done on the interface of the electronic control system and to show how we can do them.

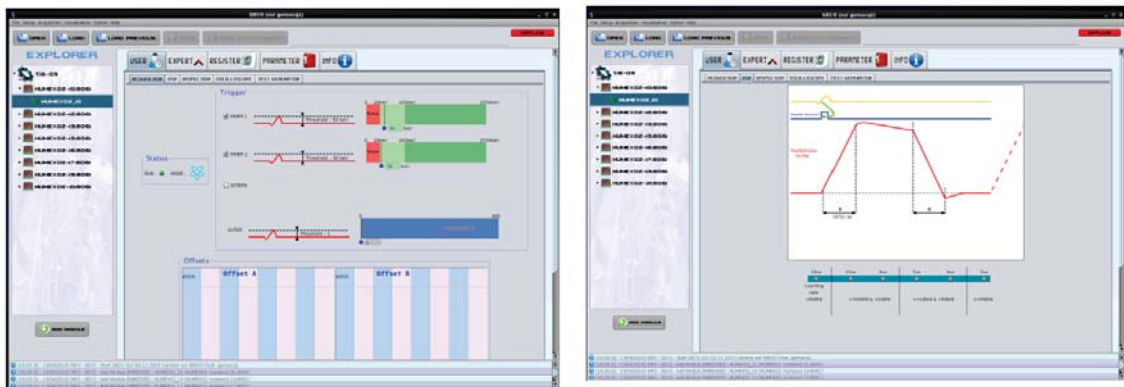


Figure 4.10. Left; NUMEXO2 trigger control panel, Right; Trapezoidal filter slope, K-parameter control panel [47]

Main control interface is shown in Figure 4.10. This interface has two main menus, the first is to open and load any of the previously saved control configurations, the second is to load a previously saved configuration that works. Five different sections can be seen, when passed to control process for each NUMEXO2, such as user, expert, register, parameter and info (Figure 4.10).

Specifically, as it is clearly visible, there are five different subsections under the user menu. Those are acquisition, DSP, inspection, oscilloscope and test generator.

In acquisition section, whether the two inner crystals of the EXOGAM2 detector that connected to each channel of the NUMEXO2 should record data depending on which triggering conditions can be determined. Or whether an external signal can be used to carry out the data recording (see the left side of Figure 4.10).

DSP section, control of k- parameter, which determines the quality of the signal proceed in the trapezoidal form, is provided. Furthermore, this parameter affects the energy resolution that represents each gamma-energy peak in the energy spectrum (see

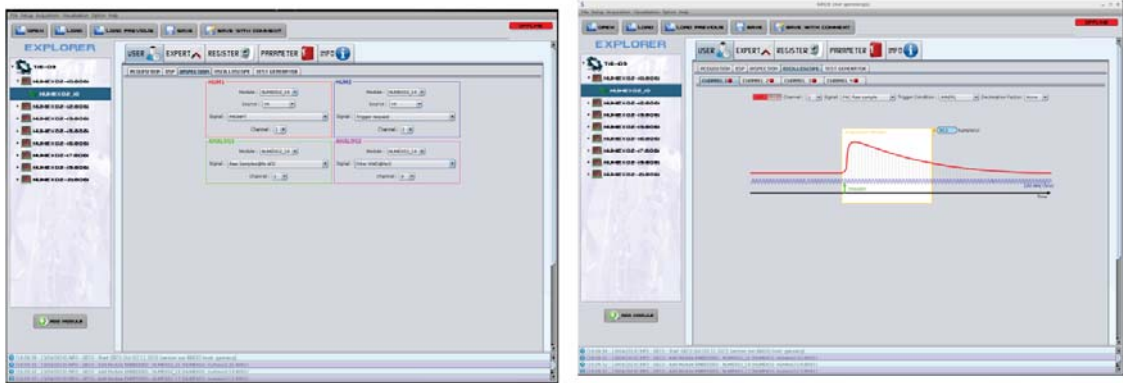


Figure 4.11. Left; inspection control panel, Right; Oscilloscope control panel [47]

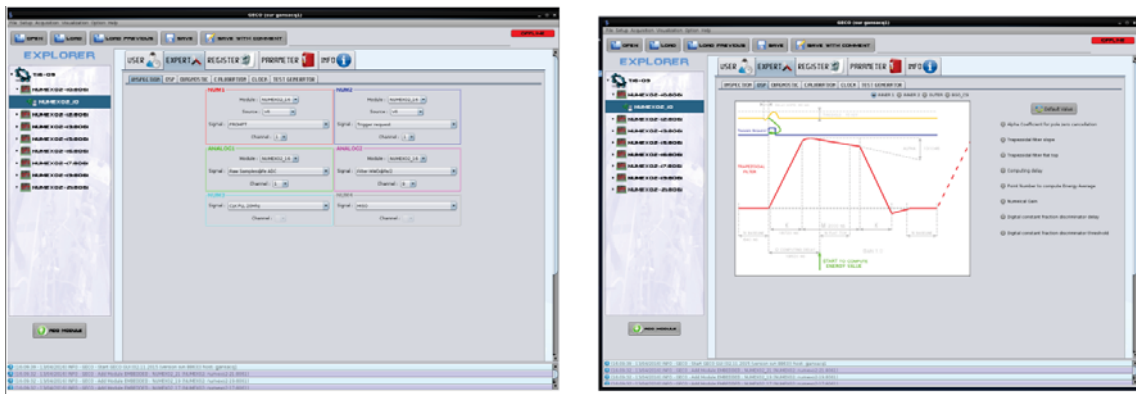


Figure 4.12. Left; Trigger timing control panel, Right; K, M ve alfa-parameters control panel [47]

the right side of Figure 4.10).

In inspection mode, the data that received from Virtex5 or Virtex6 of NUMEXO2 is determined whether recorded in either digital (Trigger mode, valid or invalid data or simple data etc.) or analog (raw data, filtered moving window etc.) mode (see the left side of Figure 4.11).

In oscilloscope mode, the signal is saved depending on which mode (raw data, trapezoidal mode etc.) or which part of the detector (inner1, inner2, external trigger etc.) it needs to be saved (see the right side of Figure 4.11).

In the expert mode on the NUMEXO2 unit, it is possible to determine whether the digital or analog modes of NUMEXO2 should process each signal received from Virtex5

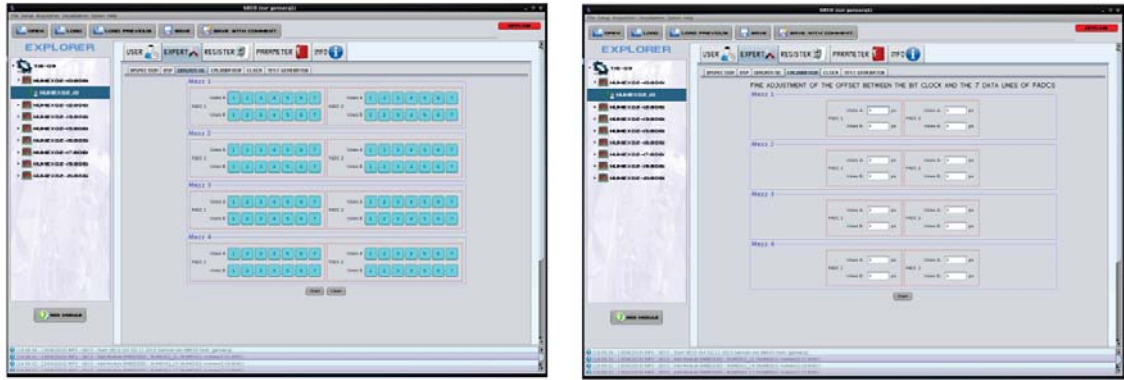


Figure 4.13. Left; FADC control panel, Right; Each FADC fine adjustment control panel [47]

or Virtex6, and which time interval it should taken (see the left side of Figure 4.12).

When the signal processed in the trapezoidal form, quality of the signal can be determined not only by the K-parameter, but also by M-parameter and the alpha-parameter. In the right side of the figure, it is possible to decide which parameter should be taken together with which option, and which detector unit is triggered according to that parameter value (see the right side of Figure 4.12).

In expert mode, control of the FADC electronic cards within NUMEXO2 can be done and their functionality can be checked (the left side of Figure 4.13). Fine tuning of the FADCs calibration can be made. Clock and test generator sections are still under development in expert mode. (the right side of Figure 4.13).

In register mode, as can be seen from the left side of Figure 4.14, if for example Virtex-6 parameter of NUMEXO2 is required to record in which mode, we can see the panel that performs control and modifies this recording value, while on the right side, when each unit within NUMEXO2 reads data It is possible to determine which format data to be readout.

Parameter which is the fourth menu in the left side of Figure 4.10, is still under development, while in info menu, there is a flow diagram that shows units in NUMEXO2, how they communicate with each other and in which order.

All these information about GECO interface are important, since controls of AGA-TA, NEDA, DIAMANT, PARIS, which are used at the international project in SPIRAL2 at GANIL, and controls of all ancillary detectors system will be performed by means of GECO. Additionally, GECO with oscilloscope mode provides data acquisition and con-

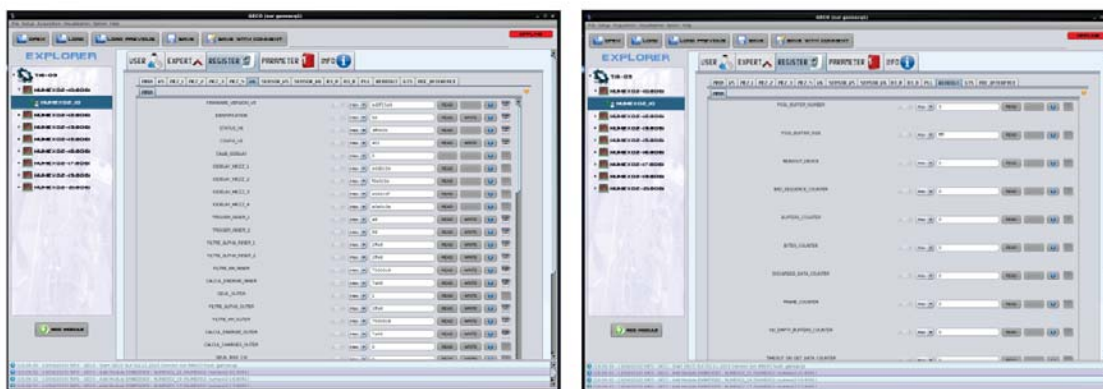


Figure 4.14. Left; Control panel of data that is acquisition in data registration within parts of NUMEXO2, Right; NUMEXO2 data readout value control panel [47]

control, GECO also makes it possible to make necessary adjustments on the devices without physically entering the test environment, since it is important to be able to control the devices in the experimental environment without physically accessible.

VIGRU is another program that is used after the experiment in order to analyze data and it is as important as GECO.

Figure 4.15 shows VIGRU interface, and graphics which is produced in different forms. While the experiment is proceeding, the VIGRU program offers the possibility to check the qualities of spectra alpha, beta and gamma rays that belong to the intended nuclei, and the spectra of whether the test data are recorded in the desired quality by making approximate measurements during the test.

VIGRU software provides the display of histograms, one-dimensional, two-dimensional and three-dimensional spectra that are suitable data formats for the experiment. Furthermore, it is a software that enables to perform intended measurements on these histograms or spectra. Thanks to the VIGRU software, the spectra, histograms that belong to each unit within each detector system can be displayed individually or collectively by means of a graphical interface and required physical and statistical measurements can be made on them. Furthermore, the most used functions are reported on the front of the interface to be friendly and useful. VIGRU can also load root histograms or Ganil Acquisition histogram

Before all these measurements or display process, calibration operations should be made and calibration coefficient should be found. For this process, To find calibration

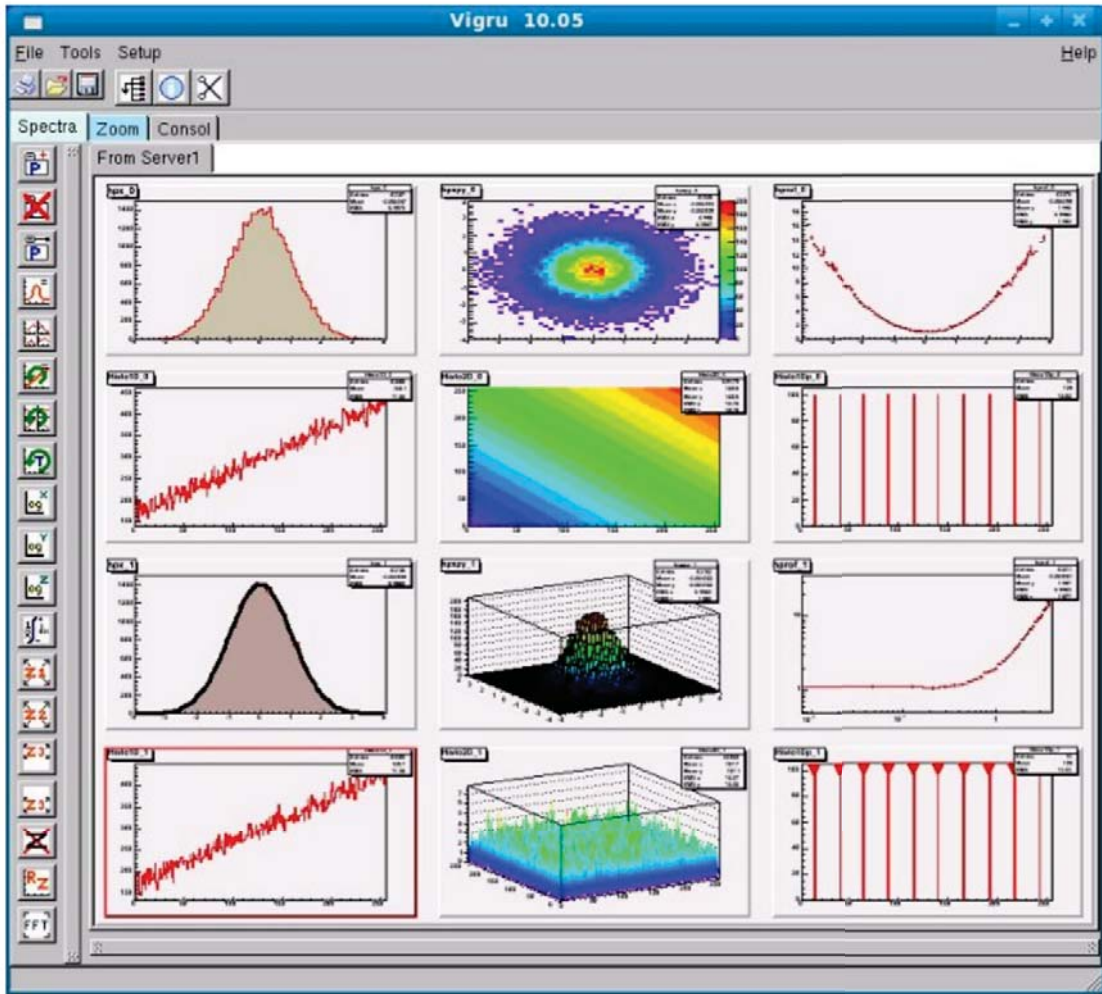


Figure 4.15. VIGRU graphical interface control panel [46]

coefficient, VIGRU provides convenience to plot and display data that are taken from the experiment.

CHAPTER 5

RESULTS

A common requirement in scientific data processing is to detect peaks in a signal and to measure their positions, heights, widths, and/or areas. By using known radioactive gamma sources an energy calibration of the detector can be performed. Before creating histograms, energy spectra or matrices that will be measured from received data, calibration coefficients analyses are necessary to make measurements before and after the experiment by using radioactive sources. Calibration coefficients should be found by making calibration for energy peaks that located two different regions and the center region by using ^{152}Eu calibration source that has intense energy peaks both low energy (100-200 keV) region and high energy (1400-1600 keV) region of detectors. Afterward, by using these calibration coefficients for each detector and crystal in course of the experiment, the signals that detected are correctly recorded.

We performed an experiment by using four NUMEXO2 digitizers and two EXOGAM2 detectors. GECO and VIGRU programs were made the check in order to save the data. All the experiment data was saved as digital for the first time in our calibration process. Before the actual nuclear experiment with the beam and target is carried out, calibration process should be done. In order to obtain such calibration coefficient and examine the performance of the NUMEXO2 digitizer, an actual on beam experiment was carried out in April 2016, using the ^{58}Ni beam at $E_{beam} \approx 180\text{MeV}$ and ^{58}Ni target on 518 mg/cm^2 thick. During this experiment four NUMEXO2 digitizer were used with two EXOGAM2 detectors. Before taking real data from this nuclear reaction ^{152}Eu radioactive source was used in order to obtain calibration coefficients of each crystal used in EXOGAM2 detectors.

To analyse this digital data, GRU, VIGRU, GECO and ROOT programs were used with the computer that has Linux operating system. Intense energy peaks in energy spectrum made peak fitting process with ROOT program by using ^{152}Eu calibration source. Therefore, after peak fitting process of energy signals, these energy signals that obtained from NUMEXO2 will be located in the right position. More clearly, Table 5.1 gives commonly observed gamma energies of ^{152}Eu that can be obtained from the atomic database [48]. In this study our interested energy levels are both 344.785 keV and 1.408.006 keV. Because these energy values are two extreme energy values. They may show different

Table 5.1. Intense energy value of ^{152}Eu radioactive calibration source

<i>Energy (keV)</i>
121.782
344.785
778.904
964.079
1.085.869
1.112.074
1.408.006

energy resolution values of crystals in these energy.

Table 5.2 shows the results that are measured. These results are obtained by using the fitting process that belongs to energy spectra of ^{152}Eu calibration source. Figure 5.7 and Figure 5.8 shows also how we obtain these mean energy values.

In Figure 5.1 shows that after peaks fitting process of ^{152}Eu radioactive calibration source at 344.785 keV and at 1.408.006 keV, mean energy values obtained for the second crystal of the first of EXOGAM2 detectors.

The positions of the peaks in the measured spectra are obtained from a Gaussian fit, with linear or constant offset. By using mean energy values obtained from peak fitting process, correction coefficients that were got from each crystal were found by turning these mean energy values into values in Table 5.1. These coefficients found by using scatter diagram, thus the scatter diagram gave the line equation. Coefficients of the line equation gave the calibration coefficients to us. Top left-hand corner in Figure 5.2 shows these correction coefficients.

As we mentioned before, we used two EXOGAM2 detector which means that totally eight germanium crystals are used. By using calibration coefficient, the energy values of ^{152}Eu radioactive calibration source in the spectrum was ensured that being in energy values in Table 5.1. To show how calibration process works, energy spectra that used calibration coefficients are shown in left side of Figure 5.3, while energy spectra that

Table 5.2. Measured energy value of ^{152}Eu radioactive calibration source

B110A Crystal (keV)	B110B Crystal (keV)	B112A Crystal (keV)	B112B Crystal (keV)	B113A Crystal (keV)	B113B Crystal (keV)	B116B Crystal (keV)	B116B Crystal (keV)
128.000	131.818	—	—	129.909	125.563	146.763	118.800
355.090	350.000	355.454	339.636	365.454	353.096	358.000	342.000
800.360	780.000	779.818	765.454	832.000	798.727	809.090	777.000
1002.540	980.363	961.090	962.545	1025.454	990.363	1001.818	958.000
1130.180	1105.454	1082.000	1081.090	1154.181	1127.090	1128.727	1075.636
1134.180	1134.909	1109.096	1109.272	1181.272	1129.272	1155.090	1104.909
1466.180	1430.000	1403.090	1403.090	1495.272	1444.181	1462.363	1398.909

used without calibration coefficients are shown in right side of Figure 5.3 for first four crystals (crystal 1, crystal-2, crystal-3, crystal-4 in the range of 0-500 keV). Figure 5.4 shows second four crystals of EXOGAM2 detector (in the range of 0-500 keV). While Figure 5.5 shows first four crystals of EXOGAM2 detector (crystal-5, crystal-6, crystal-7, crystal-8 in the range of 500-1500), Figure 5.6 shows second four crystals of EXOGAM2 detector (in the range of 500-1500).

One of each energy was selected from high and low energy spectrum by using Figure 5.3, 5.4, 5.5, 5.6 that obtained by using calibration source. Therefore, energy resolution was analyzed for each of crystals by using energy spectrum. For energy resolution, related energy peaks were analyzed for each of crystal. These analyze shown in Figure 5.7 and 5.8. We used ROOT software for fitting process. In Figure 5.7 show the result of peak fitting processes for 344.785 keV energy value, while In Figure 5.8 show the result of peak fitting process for 1.408.006 keV.

After the energy peak fitting process, as we mentioned in Chapter 3, energy resolution was calculated as FWHM. Energy resolution values for each crystal (344.785 keV and 1.408.006 keV) was found by using obtained energy values and these results given in Table 5.3. HPGe crystals should have 2.1-2.4 energy resolution, these values are defined as the good resolution for HPGe detectors. The performance of HPGe detectors depends on the operation temperature of crystal and electronics, therefore the temperature of the

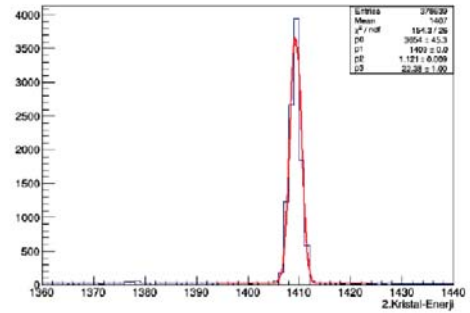
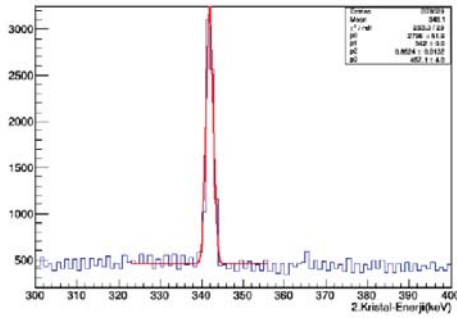


Figure 5.1. Peaks fitting process of ^{152}Eu radioactive calibration source at 344.785 keV and at 1.408.006 keV

detector can affect the energy resolution, too. For this reason, sometimes energy resolution values for each crystal can show an alteration.

Table 5.3. Energy resolution values of the EXOGAM2 detector crystals

Crystal Name	FWHM for Low Energy Region (344.785 keV)	FWHM for High Energy Region (1408.006 keV)
1) B110A	2.087	2.687
2) B110B	2.026	2.634
3) B112A	2.004	2.573
4) B112B	3.168	2.938
5) B113A	2.411	2.670
6) B114B	2.409	2.677
7) B116A	2.813	3.410
8) B116B	2.616	4.051

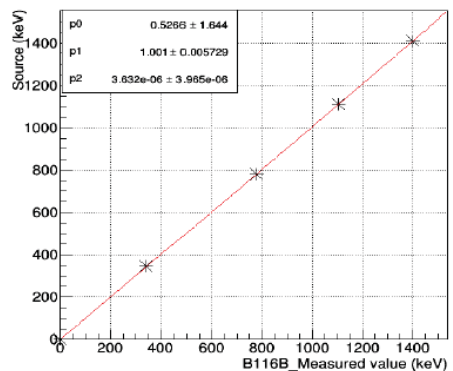
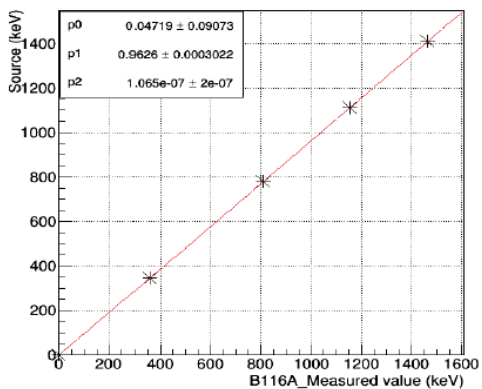
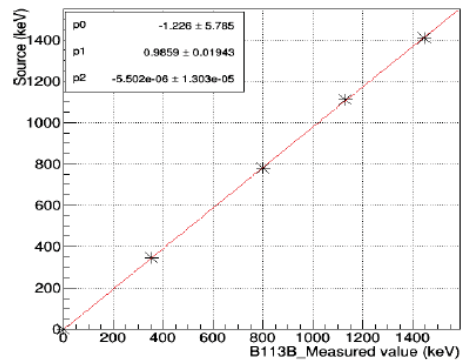
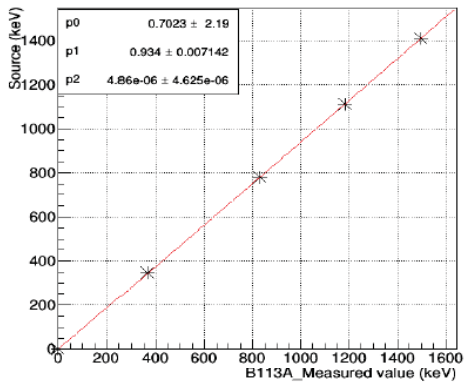
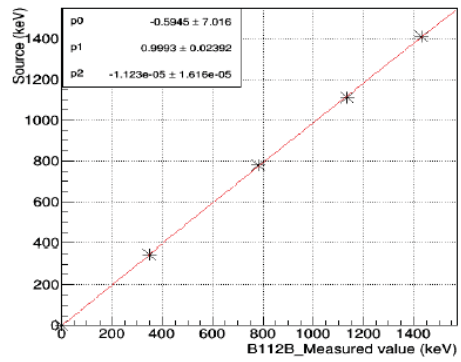
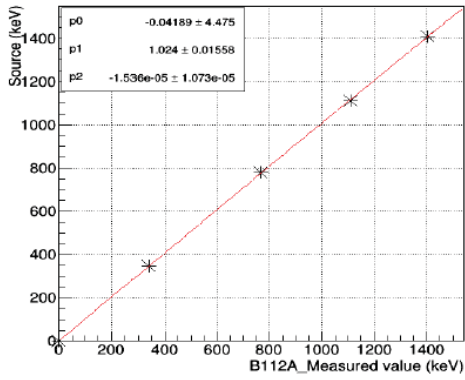
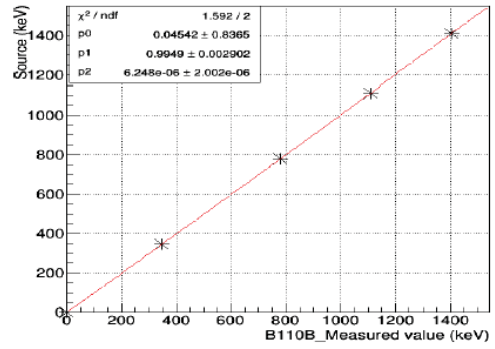
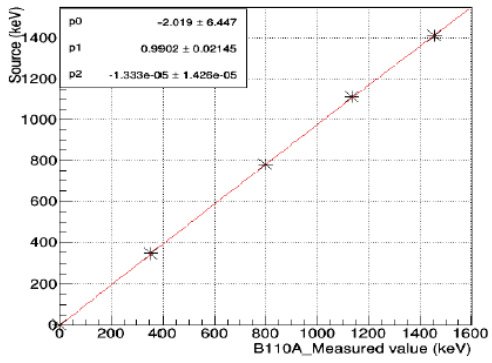


Figure 5.2. Correction coefficients obtained by using energy fitting process by using each of crystals for two EXOGAM2 detectors

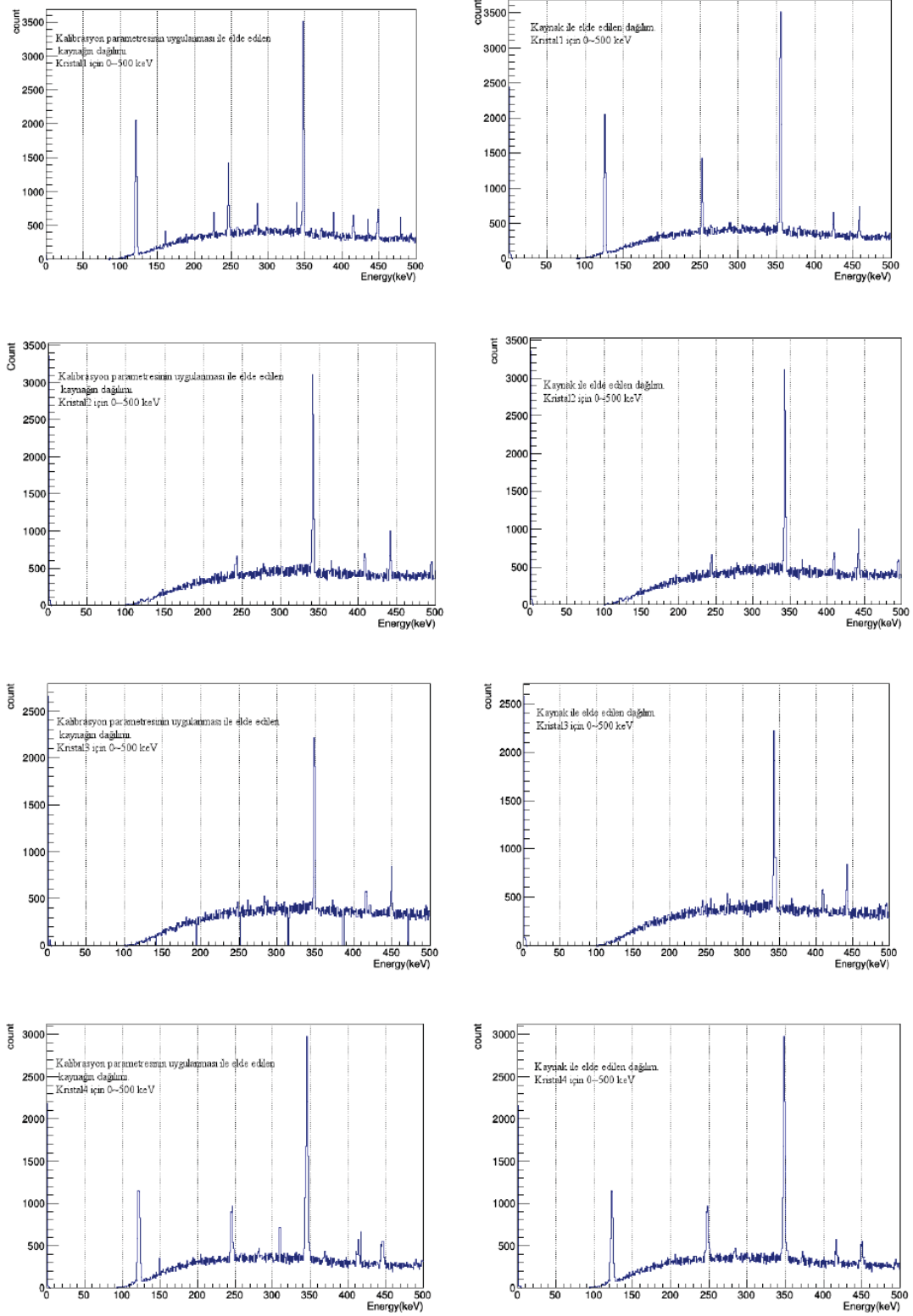


Figure 5.3. First four crystals of EXOGAM2 energy spectrum (in the range of 0-500 keV), the left side shows energy spectra that used calibration coefficients and the right side shows energy spectra that used without calibration coefficients

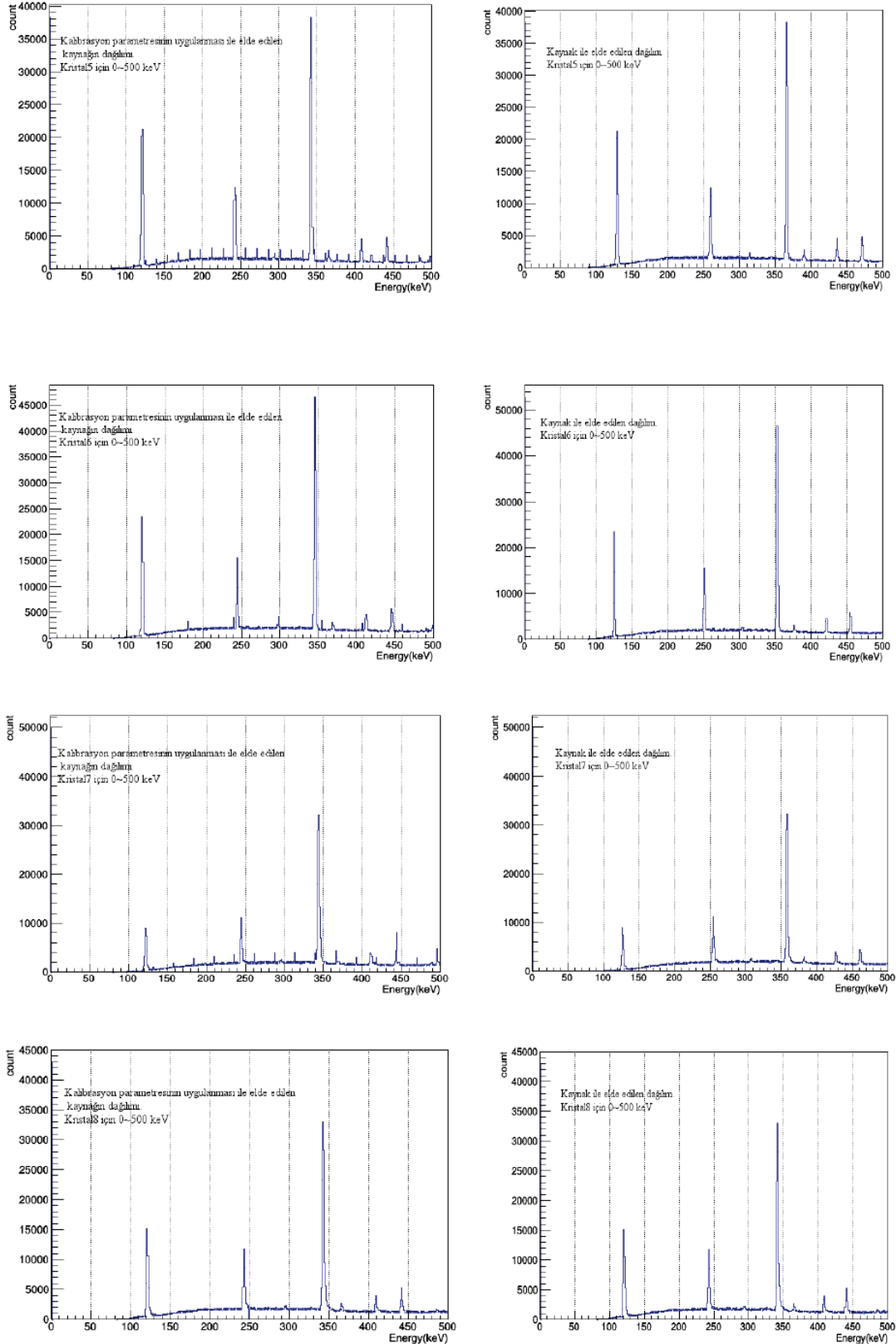


Figure 5.4. Second four crystals of EXOGAM2 energy spectrum (in the range of 0-500 keV), the left side shows energy spectra that used calibration coefficients and the right side shows energy spectra that used without calibration coefficients

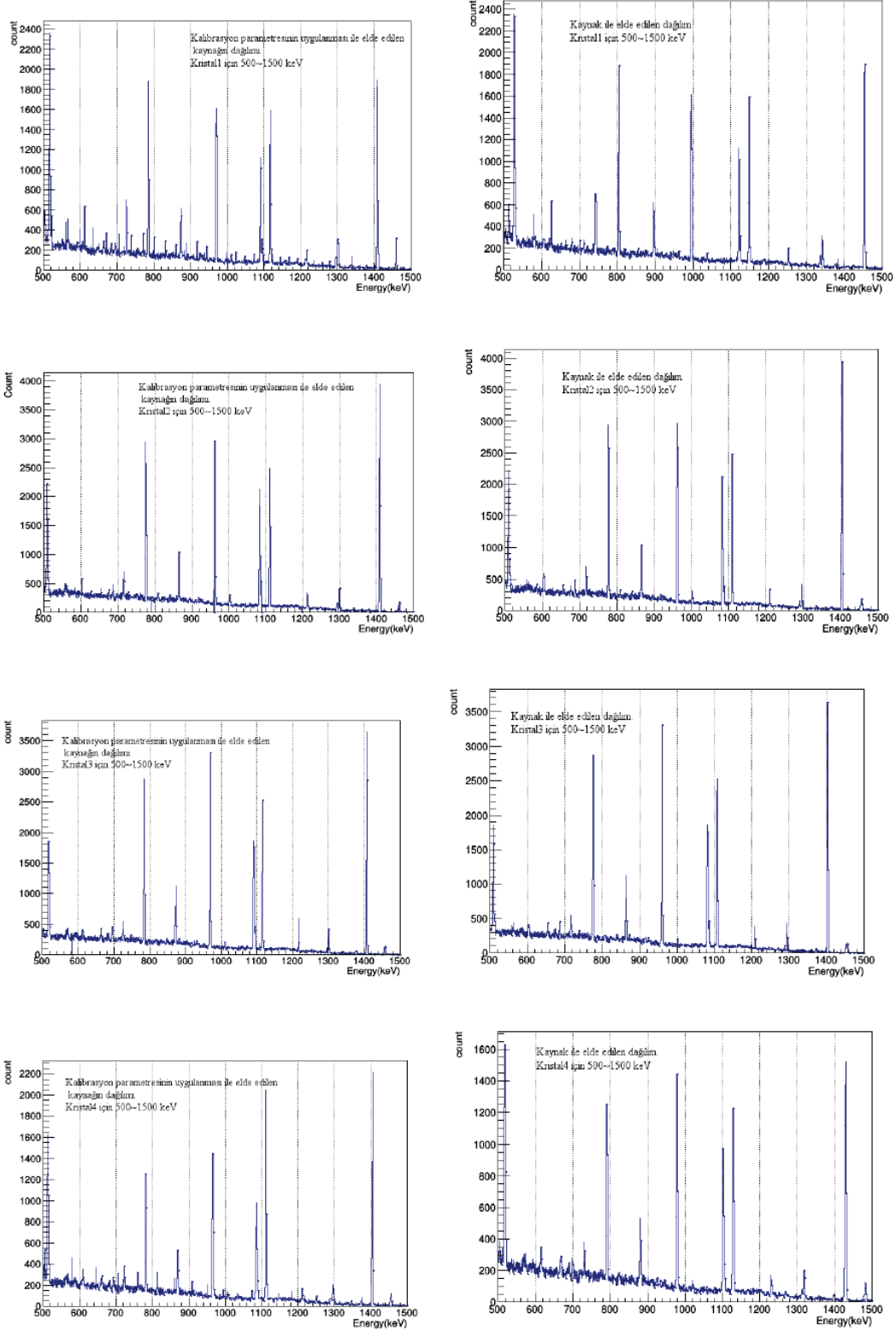


Figure 5.5. First four crystals of EXOGAM2 energy spectrum (in the range of 500-1500 keV), the left side shows energy spectra that used calibration coefficients and the right side shows energy spectra that used without calibration coefficients

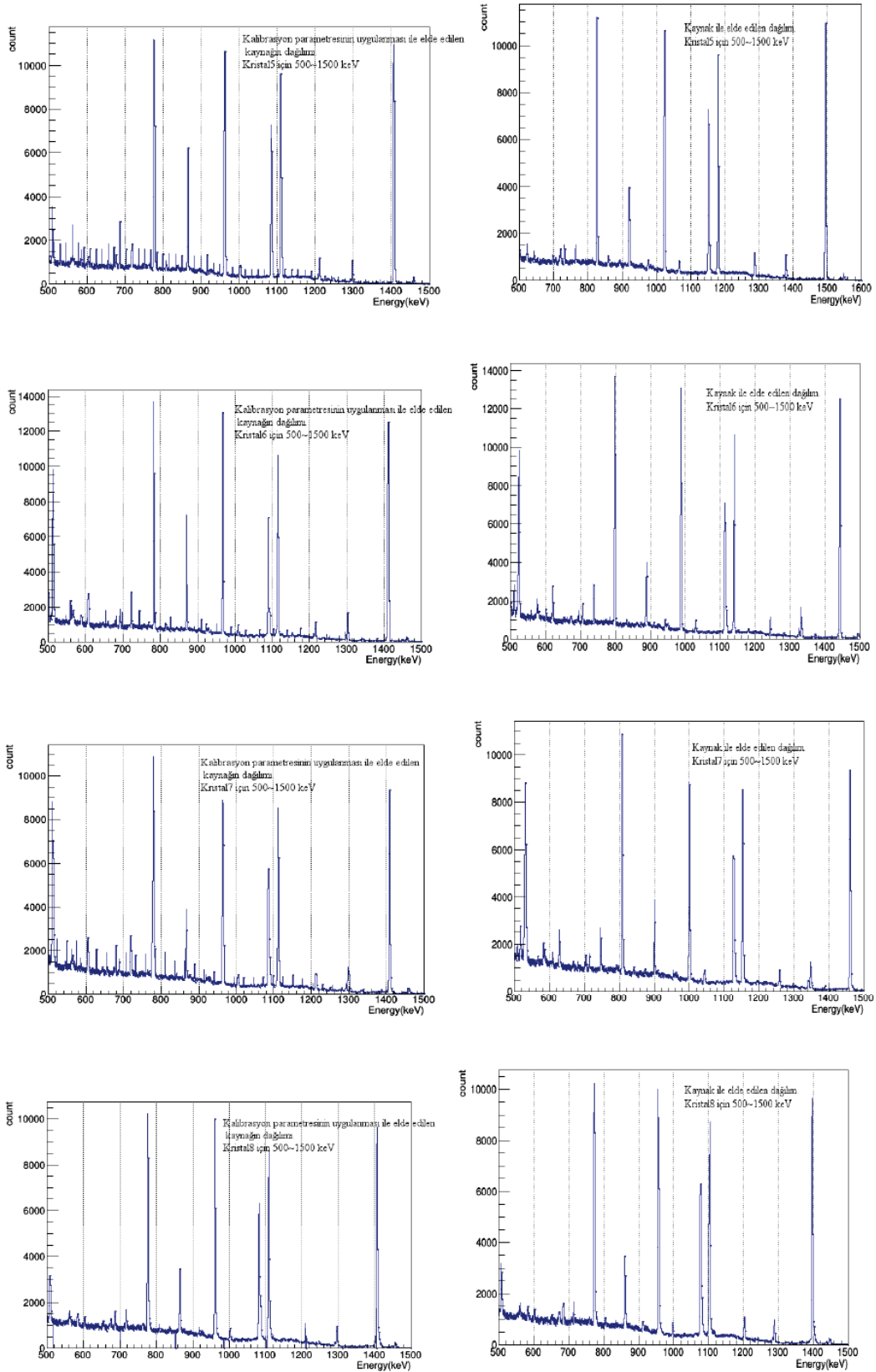


Figure 5.6. Second four crystals of EXOGAM2 energy spectrum (in the range of 500-1500 keV), the left side shows energy spectra that used calibration coefficients and the right side shows energy spectra that used without calibration coefficients

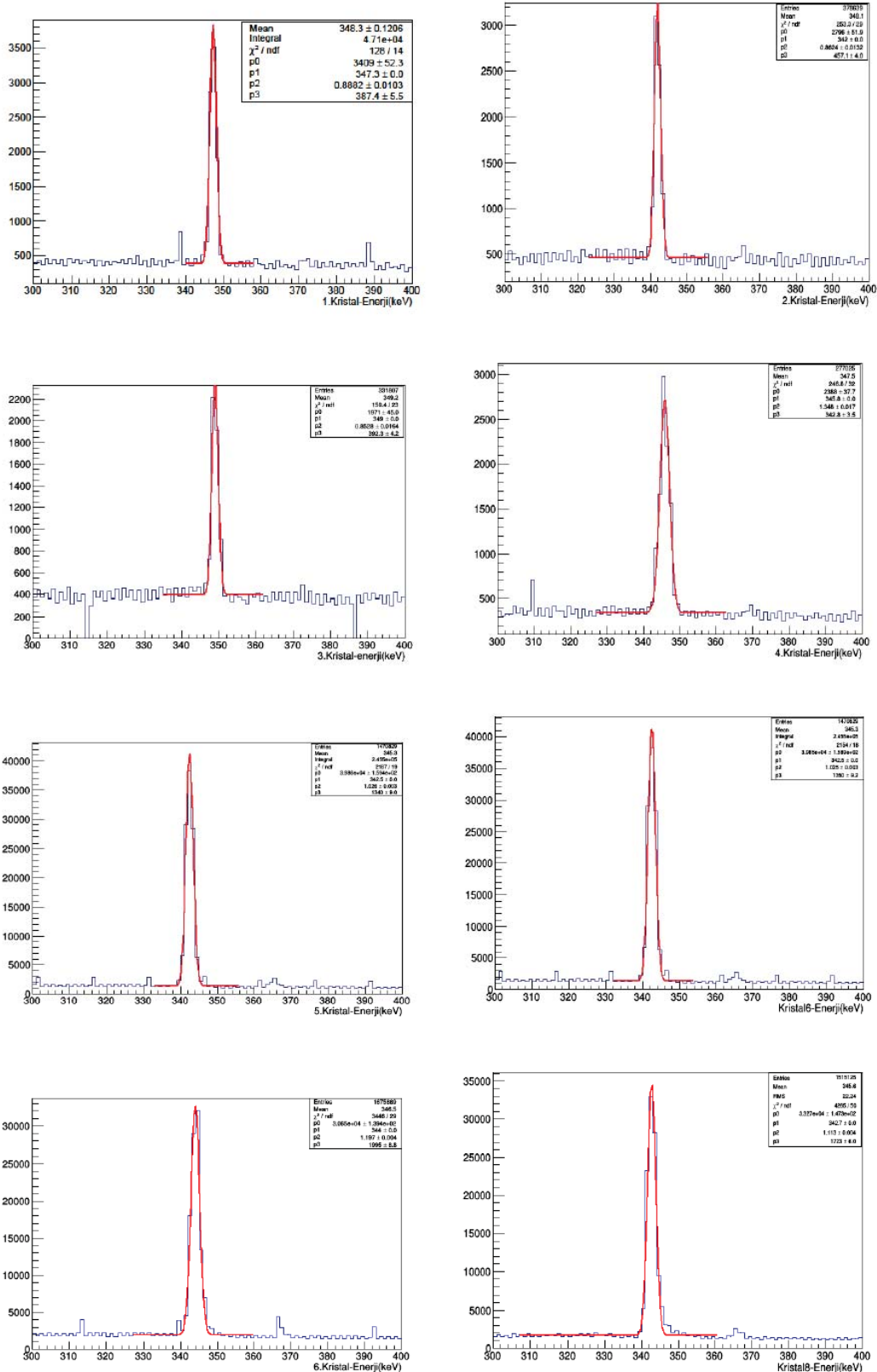


Figure 5.7. Results of energy fitting process of each EXOGAM crystal at 344.785 keV

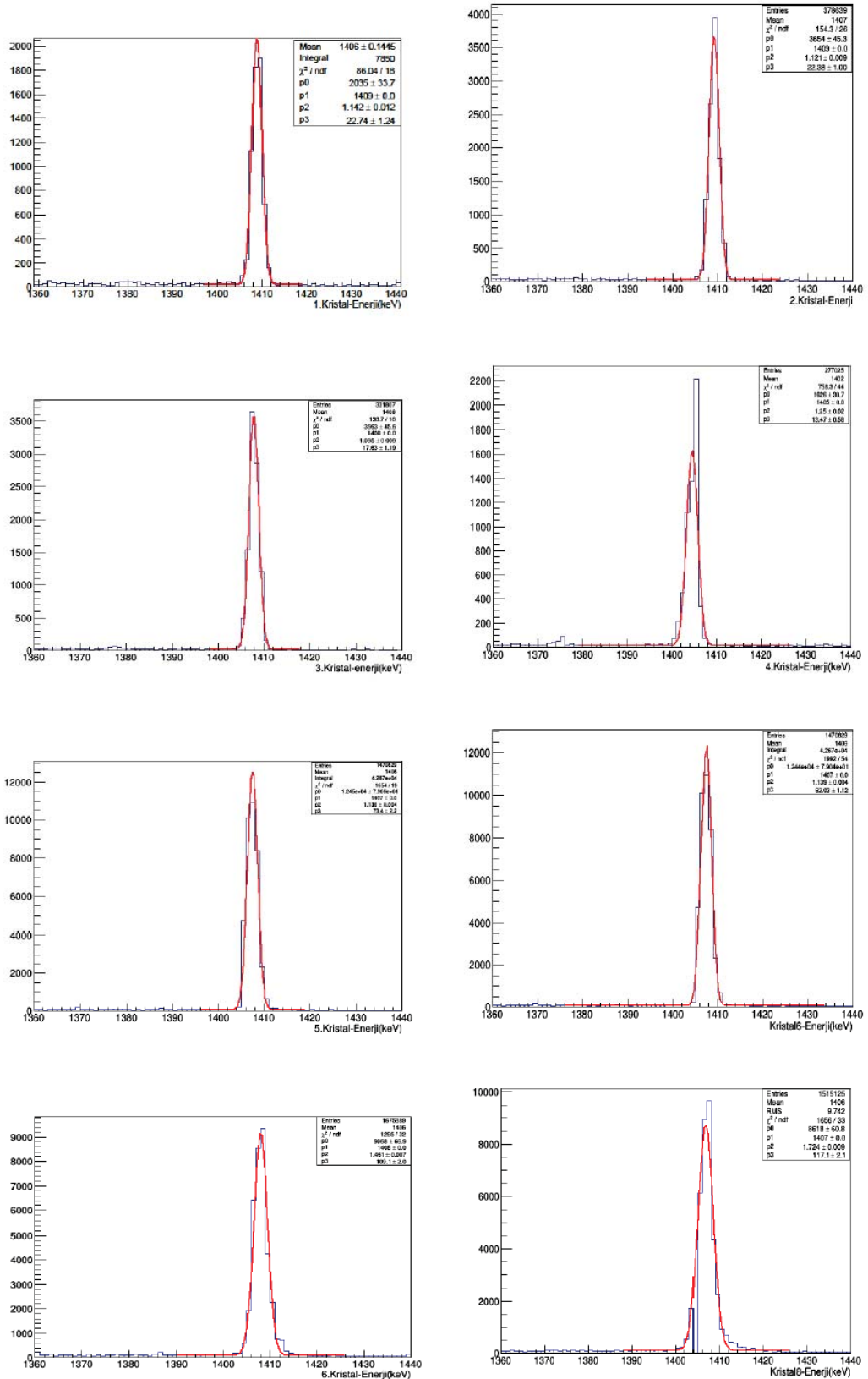


Figure 5.8. Results of energy fitting process of each EXOGAM crystal at 1408.006 keV

CHAPTER 6

CONCLUSION

One of the main goals of this thesis was to use the NUMEXO2 digitizer with EXOGAM2 array during the experiment in order to obtain the performance of NUMEXO2 which will be one of the most important device used with EXOGAM2 and with other detector systems namely, NEDA neutron detector, PARIS calorimeter to discover new properties of exotic nuclei. In order to improve the performance of EXOGAM2 array, currently used analog electronic replaced with NUMEXO2 successfully. The NUMEXO2 digital electronic has data transfer rate of 100~200 MHz ($10^8 \sim 2 \cdot 10^8 Hz$) while the analog electronic has data transfer rate of 10~20 kHz ($10^4 \sim 2 \cdot 10^4 Hz$). As can be seen from data transfer rates, NUMEXO2 has better data transfer rate as ten thousand times then analog electronic.

In order to examine the performance of the NUMEXO2 digitizer, an actual on beam experiment was carried out in April 2016, using the ^{58}Ni beam at $E_{beam} \approx 180 MeV$ and ^{58}Ni target on $518 mg/cm^2$ thick. During this experiment four NUMEXO2 digitizer were used with two EXOGAM2 detectors. Before taking real data from this nuclear reaction ^{152}Eu radioactive source was used in order to obtain calibration coefficients of each crystal used in EXOGAM2 detectors. Table 5.2 shows the energy resolution for low (344.785 keV) and high (1408.006 keV) energy peaks are chosen for EXOGAM2 crystals. Our results are demonstrated that resolution values at the low energy level and at the high energy level are getting worse as it is expected and this is related to the characteristic properties in the high energy efficiency of the detectors. Especially, the resolution of 4th, 7th and 8th crystals at low and high energy level shows the unexpected results which need further examination in the future by testing this detector with other experiments.

As a result, in this study, we showed the performance of NUMEXO2 for its energy resolution analyses. Moreover, we observed that the NUMEXO2 digitizer was worked satisfactorily during the experiment and enabled us to have first good data set from a test experiment.

REFERENCES

- [1] G De Angelis, A Bracco, and D Curien. The euroball gamma ray detector array. *euro-physics news*, 34(5):181–185, 2003.
- [2] FS Goulding, DA Landis, N Madden, M Maier, and H Yaver. Gammasphere. overview of detector and signal processing system. In *Nuclear Science Symposium and Medical Imaging Conference Record, 1995., 1995 IEEE*, volume 1, pages 432–436. IEEE, 1995.
- [3] J Eberth, G Pascovici, HG Thomas, N Warr, D Weißhaar, D Habs, P Reiter, P Thierolf, D Schwalm, C Gund, et al. Miniball: A gamma-ray spectrometer with position-sensitive ge detectors for nuclear structure studies at rex-isolde. In *AIP Conference Proceedings*, volume 656, pages 349–356. AIP, 2003.
- [4] G. de France. Exogam detectors. Retrieved March 27, 2017, from <http://pro.ganil-spiral2.eu/laboratory/detectors/exogam/exogam-detectors>.
- [5] S Akkoyun, Alejandro Algora, B Alikhani, F Ameil, G De Angelis, L Arnold, A Astier, Ayşe Ataç, Y Aubert, C Aufranc, et al. Agata advanced gamma tracking array. *Nuclear Instruments and Methods in Physics Research Section A: Accelerators, Spectrometers, Detectors and Associated Equipment*, 668:26–58, 2012.
- [6] CW Beausang. Greta: the gamma-ray energy-tracking array. status of the development and physics opportunities. *Nuclear Instruments and Methods in Physics Research Section B: Beam Interactions with Materials and Atoms*, 204:666–670, 2003.
- [7] PT Greenlees. on behalf of the jurogam and great collabs. *Nucl. Phys. A*, 787:507c, 2007.
- [8] DG Sarantites, W Reviol, CJ Chiara, RJ Charity, LG Sobotka, M Devlin, M Furlotti, OL Pechenaya, J Elson, P Hausladen, et al. Neutron shell: a high efficiency array of neutron detectors for γ -ray spectroscopic studies with gammasphere. *Nuclear Instruments and Methods in Physics Research Section A: Accelerators, Spectrometers, Detectors and Associated Equipment*, 530(3):473–492, 2004.

- [9] J. Nyberg. Neutron wall. Retrieved March 31, 2017, from <http://egpworkshop.in2p3.fr/docs/Talks-Mardi/nwall-jn.pdf>, 27-30 May 2008.
- [10] Ö Skeppstedt, HA Roth, L Lindström, R Wadsworth, I Hibbert, N Kelsall, D Jenkins, H Grawe, M Górska, M Moszyński, et al. The euroball neutron wall—design and performance tests of neutron detectors. *Nuclear Instruments and Methods in Physics Research Section A: Accelerators, Spectrometers, Detectors and Associated Equipment*, 421(3):531–541, 1999.
- [11] J.J. Valiente-Dobon. Neda - neutron detector array. Retrieved May 10, 2016, from <http://www.mi.infn.it/WSBormio-Milano2012/Doc/TALK/Dobon-Bormio12-web.pdf>, 22-25 February 2012.
- [12] G Jaworski, M Palacz, Johan Nyberg, G De Angelis, G De France, A Di Nitto, J Egea, MN Erduran, S Ertürk, E Farnea, et al. Monte carlo simulation of a single detector unit for the neutron detector array neda. *Nuclear Instruments and Methods in Physics Research Section A: Accelerators, Spectrometers, Detectors and Associated Equipment*, 673:64–72, 2012.
- [13] D. Mengoni. Status of the trace array. In *SPES Workshop*, 2010.
- [14] BM Nyakò et al. Performance of the diamant detector at ganil and plans for improvements. *ATOMKI laboratory: for the DIAMANT collaboration,(unpublished)*, 2007.
- [15] I Antón, G Sala, JC Arboiro, J Monedero, and P Valera. Effect of the optical performance on the output power of the euclides array. In *Proceedings of the 16th Photovoltaic Solar Energy Conference and Exhibition*, volume 3, pages 2225–2228, 2000.
- [16] Kenneth S Krane and David Halliday. *Introductory nuclear physics*, volume 465. Wiley New York, 1988.
- [17] Alejandro Sonzogni. Nndc chart of nuclides. In *International Conference on Nuclear Data for Science and Technology*, pages 105–106. EDP Sciences, 2007.
- [18] Retrieved June 17, 2016, from <http://www.yorku.ca/eye/spectru.htm>.

- [19] Nicholas Tsoulfanidis. *Measurement and detection of radiation*. CRC press, 2013.
- [20] Ian Rittersdorf. Gamma ray spectroscopy. *Nuclear Engineering & Radiological Sciences*, pages 18–20, 2007.
- [21] Francisco Javier Egea Canet. *Design, verification and integration of a fast digitizer for nuclear structure experiments. Application to EXOGAM and NEDA detectors*. PhD thesis, Universty of Valencia, September 2015.
- [22] Primary photon contribution. Retrieved April 14, 2016 from <https://www.nucleonica.com/wiki/index.php?title=Help>
- [23] TW Crane and MP Baker. Chapter 13,neutron detectors. *Passive Nondestructive Assay of Nuclear Materials*, edited by TD Reilly, N. Ensslin, and HA Smith, US Nuclear Regulatory Commission NUREG/CR-5550, 1991.
- [24] P Rinard. 12-neutron interactions with matter. Retrieved January 23, 2017, from <http://www.fas.org/sgp/othergov/doe/lanl/lib-www/la-pubs/00326407.pdf>.
- [25] Retrieved September 28, 2016, from <https://www.halbleiter.org/en/fundamentals/conductors-insulators-semiconductors/>.
- [26] Retrieved October 25, 2016, from <http://freeengineeringnotes.blogspot.com.tr/2009/01/n-type-semiconductor.html>.
- [27] Retrieved October 25, 2016, from <http://freeengineeringnotes.blogspot.com.tr/2009/01/p-type-semiconductor.html>.
- [28] RD Baertsch and RN Hall. Gamma ray detectors made from high purity germanium. *IEEE Transactions on Nuclear Science*, 17(3):235–240, 1970.
- [29] WL Hansen. High-purity germanium crystal growing. *Nuclear Instruments and Methods*, 94(2):377–380, 1971.
- [30] J Llacer and HW Kraner. Neutron damage and annealing in high purity germanium radiation detectors. *Nuclear Instruments and Methods*, 98(3):467–475, 1972.

- [31] Glenn F Knoll. *Radiation detection and measurement*. John Wiley & Sons, 2010.
- [32] Jr. Hastings A. Smith and Marcia Lucas. Gamma-ray detectors. Retrieved October 12, 2016, from <http://www.lanl.gov/orgs/n/n1/panda/00326398.pdf>.
- [33] J Eberth and J Simpson. From ge (li) detectors to gamma-ray tracking arrays—50 years of gamma spectroscopy with germanium detectors. *Progress in Particle and Nuclear Physics*, 60(2):283–337, 2008.
- [34] HW Kraner. Fast neutron damage in germanium detectors. *IEEE Transactions on Nuclear Science*, 27(1):217–234, 1980.
- [35] Richard H Pehl. Radiation damage of germanium detectors. *Lawrence Berkeley National Laboratory*, 2011.
- [36] F Azaiez. Exogam: a γ -ray spectrometer for radioactive beams. *Nuclear Physics A*, 654(1):1003c–1008c, 1999.
- [37] Sébastien Alexandre Adrien Gros. *Characterisation of an EXOGAM clover germanium detector*. University of Liverpool, 2005.
- [38] J Simpson, F Azaiez, G De France, J Fouan, J Gerl, R Julin, W Korten, PJ Nolan, BM Nyako, G Sletten, et al. The exogam array: a radioactive beam gamma-ray spectrometer. *Acta Physica Hungarica, New Series, Heavy Ion Physics*, 11:159–188, 2000.
- [39] S Levinson, A Israelashvili, O Shachal, O Pelled, and U German. Background reduction of a hpge-bgo anti-compton system and its application to soil contamination monitoring. 2004.
- [40] I Lazarus. The exogam electronics system architecture. Retrieved April 20, 2017, from <http://npg.dl.ac.uk/documents/edoc405/System-Arch-v05.htm>.
- [41] M Tripon. Exogam2 technical specifications, 2012.
- [42] FJ Egea Canet et al. A new front-end high-resolution sampling board for the new-generation electronics of exogam2 and neda detectors. *IEEE Transactions on Nu-*

clear Science, 62(3):1056–1062, 2015.

- [43] Francisco Javier Egea, Enrique Sanchis, Vicente González, Andres Gadea, Jose María Blasco, Diego Barrientos, JJ Valiente Dobón, Michel Tripou, Abderrahman Boujrad, Charles Houarner, et al. Design and test of a high-speed flash adc mezzanine card for high-resolution and timing performance in nuclear structure experiments. *IEEE Transactions on Nuclear Science*, 60(5):3526–3531, 2013.

- [44] F Saillant. Upgrade acquisition/data center. In *GANIL-SPIRAL2 Week 2014*, 2014.

- [45] Rene Brun and Fons Rademakers. Root an object oriented data analysis framework. *Nuclear Instruments and Methods in Physics Research Section A: Accelerators, Spectrometers, Detectors and Associated Equipment*, 389(1-2):81–86, 1997.

- [46] Visualize ganil root utilities. Retrieved March 27, 2017, from <http://wiki.ganil.fr/gap/wiki/Documentation/Gru/Vigru>.

- [47] F. Saillant. Software developments. Retrieved April 30, 2017, from <http://w3.atomki.hu/numex02/talks>, November 2016.

- [48] IAEA. nuclide live-chart. Retrieved October 25, 2016, from <https://www-nds.iaea.org/relnsd/vcharthtml/VChartHTML.html>.